Chemical Geology 615 (2023) 121203

Contents lists available at ScienceDirect

Chemical Geology

journal homepage: www.elsevier.com/locate/chemgeo

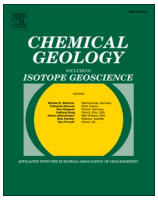

Sedimentary molybdenum and uranium: Improving proxies for deoxygenation in coastal depositional environments

K. Mareike Paul [a,*,1], Niels A.G.M. van Helmond [b], Caroline P. Slomp [b], Sami A. Jokinen [c], Joonas J. Virtasalo [c], Helena L. Filipsson [d], Tom Jilbert [a,1]

[a] Aquatic Biogeochemistry Research Unit, Ecosystems and Environment Research Program, Faculty of Biological and Environmental Sciences, University of Helsinki, Helsinki, P.O. Box 65 (Viikinkaari 1), FI-00014, Finland
[b] Department of Earth Sciences, Faculty of Geosciences, Utrecht University, Utrecht 3584, CB, the Netherlands
[c] Marine Geology, Geological Survey of Finland (GTK), Espoo, P.O. Box 96, FI-02151, Finland
[d] Department of Geology, Lund University, Lund 223 62, Sweden

ARTICLE INFO

Editor: Dr. Karen Johannesson

Keywords:
Hypoxia
Enrichment factor
Redox-sensitive
Trace metal
Coastal Sea

ABSTRACT

Sedimentary molybdenum (Mo) and uranium (U) enrichments are widely used to reconstruct changes in bottom water oxygen conditions in aquatic environments. Until now, most studies using Mo and U have focused on restricted suboxic-euxinic basins and continental margin oxygen minimum zones (OMZs), leaving mildly reducing and oxic (but eutrophic) coastal depositional environments vastly understudied. Currently, it is unknown: (1) to what extent Mo and U enrichment factors (Mo- and U-EFs) can accurately reconstruct oxygen conditions in coastal sites experiencing mild deoxygenation, and (2) to what degree secondary (depositional environmental) factors impact Mo- and U-EFs. Here we investigate 18 coastal sites with varying bottom water redox conditions, which we define by means of five "redox bins", ranging from persistently oxic to persistently euxinic, from a variety of depositional environments. Our results demonstrate that Mo- and U-EF-based redox proxies and sedimentary Mo and U contents can be used to differentiate bottom water oxygen concentration among a range of modern coastal depositional environments. This is underpinned by the contrasting EFs of Mo and U along the redox gradient, which shows a substantial difference of Mo-EFs between redox bins 3–5 (ir/regularly suboxic – ir/regularly dysoxic – persistently oxic) and of U-EFs between redox bins 1–2 (persistently euxinic – ir/regularly euxinic). Surprisingly, we observe comparatively low redox proxy potential for U in environments of mild deoxygenation (redox bins 3–5). Further, we found that secondary factors can bias Mo-and U-EFs to such an extent that EFs do not reliably reflect bottom water redox conditions. We investigate the impact of limited Mo sedimentary sequestration in sulfidic depositional environments (i.e., the "basin reservoir effect", equilibrium with $FeMoS_4$), Fe/Mn-(oxy)(hydr)oxide "shuttling", oxidative dissolution, the sulfate methane transition zone in the sediment, sedimentation rate, and the local Al background on Mo- and U-EFs.

1. Introduction

Vast coastal areas are suffering from low "bottom water" dissolved oxygen (O_2) concentrations (e.g., Diaz and Rosenberg, 2008; Rabalais et al., 2010; Breitburg et al., 2018). Terminology and thresholds for quantifying O_2 depletion have been widely discussed in literature and they differ between biological and sedimentological studies (e.g., Tyson and Pearson, 1991; Diaz and Rosenberg, 1995; Levin et al., 2009; Naqvi et al., 2010). A recent review of redox thresholds for sedimentary environments (Algeo and Liu, 2020) suggests a four-stage scheme to classify O_2 depletion (Table 1), on which the redox classification used in this study is based on. The spread of coastal deoxygenation is strongly linked to human-induced non-climatic (e.g., eutrophication) and climatic impacts (e.g., temperature rise), which enhance organic matter production and degradation, and water mass stratification (Helly and Levin, 2004; Diaz and Rosenberg, 2008; Bindoff et al., 2019). Deoxygenation leads to a stepwise decrease in benthic fauna abundance, diversity and biomass (Diaz and Rosenberg, 1995). Progress in monitoring

* Corresponding author.
E-mail address: mareike.paul@helsinki.fi (K.M. Paul).
[1] Present address: Faculty of Science, Department of Geography and Geosciences, University of Helsinki, P.O 64 (Gustaf Hällströmin katu 2), FI-00014, Finland.

https://doi.org/10.1016/j.chemgeo.2022.121203
Received 23 June 2022; Received in revised form 21 September 2022; Accepted 2 November 2022
Available online 7 November 2022

Table 1
Four-stage scheme for deoxygenation classification. For details see original publication (Algeo and Li, 2020). Oxygen concentrations in μM were taken from Algeo and Liu (2020). The redox facies "suboxic" here comprises the subdivisions "suboxidized" (0–0.2–0.7 mL L^{-1} O_2) and the "subreduced" (0 mL L^{-1} O_2, 0 mL L^{-1} H_2S, known as "anoxic-ferruginous" conditions). The ~11 μM H_2S symbolizes the approximate H_2S concentration required for the "geochemical switch" (section 2).

Environmental Redox Facies	Oxygen (O_2) concentration		Hydrogen Sulfide (H_2S) concentration
	(mL L^{-1})	(μM)	(μM)
Oxic	> 0.5–2	~60–90	0
Dysoxic ("hypoxic")	0.7–0.2	~15	0
Suboxic	0	0	0
Euxinic	0	0	> 0 (~11 μM)

and research campaigns since the 1960s has identified globally around 700 hypoxic coastal areas, and an additional 230 areas that are at risk of developing hypoxia (Diaz et al., 2019). However, the estimated number of unreported hypoxic areas is assumed to exceed 700, due to regionally poor monitoring coverage, particularly in the tropical ocean (Altieri et al., 2017; Diaz et al., 2019). Even though, several areas show signs of recovery from hypoxia (Conley et al., 2011; Diaz et al., 2019), the pace at which low O_2 areas are spreading, and the severe impact on primary productivity, marine fauna, and energy and biogeochemical cycles, makes deoxygenation one of the most important drivers of change in coastal ecosystems today (Breitburg et al., 2018; Diaz et al., 2019; Bindoff et al., 2019).

At present, the spatial and temporal development of hypoxia in coastal waters is poorly understood due to incomplete environmental monitoring coverage and limited availability of existing data (Grégoire et al., 2021). Poor understanding of local depositional environments, and biogeochemical feedbacks involved in coastal marine O_2 dynamics (Keeling et al., 2010; Breitburg et al., 2018), also contribute to knowledge gaps concerning the relationship between O_2 supply, the burial efficiencies and benthic release of nutrients and major/minor elements, and redox-sensitive trace metal dynamics. New investments in global (Global Ocean Oxygen Database and Atlas *GO$_2$DAT*, Grégoire et al., 2021) and European (European Marine Observation and Data Network *EMODnet)* marine observation networks and databases of O_2 conditions, as well as improved understanding of biogeochemical processes, aim to facilitate the development of strategies to remediate coastal hypoxia (e.g., Rabalais et al., 2010; Breitburg et al., 2018).

Occurrences of hypoxia in the coastal ocean may be recorded by chemical changes in the underlying sediment, often driven by enhanced carbon loading and, consequently, modified diagenetic processes. Deoxygenation can be detected by the sedimentary enrichment of redox-sensitive trace metals, such as molybdenum (Mo) (e.g., Manheim, 1961; Curtis, 1966) and uranium (U) (e.g., Koczy et al., 1957), which are naturally sequestered from seawater. Sedimentary Mo and U have been applied as redox proxies for reconstructing deoxygenation in depositional environments over multi-million-year to millennial (e.g., Algeo and Maynard, 2004; Tribovillard et al., 2012; Jilbert and Slomp, 2013a) and multi-centennial to seasonal time scales (e.g., Manheim, 1961; Dorta and Rona, 1971; Presley et al., 1972; Hallberg, 1974; Jacobs et al., 1985; Shaw et al., 1994; Crusius et al., 1996; Adelson et al., 2001; Algeo and Lyons, 2006; Gooday et al., 2009; Bennett and Canfield, 2020). However, studies of modern depositional systems have largely focused on restricted and permanent suboxic–euxinic basins (e.g., Algeo and Lyons, 2006; Algeo and Tribovillard, 2009) and open continental seasonal or perennial O_2 minimum zones (OMZs, Bennett and Canfield, 2020), leaving less restricted coastal areas subject to temporal variability in their O_2 availability systematically understudied.

In this study, we test the applicability of existing Mo and U based redox proxies to reconstruct deoxygenation in coastal depositional environments. Here, these environments comprise marginal seas (Baltic Sea, and Black Sea, including their deeper sub-basins, and archipelagos), the German Bight, various types of fjords (along the Swedish west coast and on Svalbard) and a dammed former estuary (marine lake Grevelingen). To systematically test the applicability of Mo and U based redox proxies, we cover in the analysis coastal depositional environments capturing the full range of bottom water redox conditions, including besides strongly restricted, deep, euxinic sites, also human-impacted oxic and dysoxic coastal sites that are representative for wide areas of the coastal ocean and remain understudied in terms of trace metal redox proxies. We tackle common caveats encountered when interpreting sediment-based Mo and U redox proxies, which can bias their applicability. These include limited Mo sequestration in sulfidic depositional environments (Algeo and Lyons, 2006; van Helmond et al., 2018; Helz, 2021), particulate Fe-/Mn (oxy)(hydr)oxide "shuttling" (Crusius et al., 1996; Algeo and Tribovillard, 2009; Tribovillard et al., 2012; Scholz et al., 2013), re-oxygenation events (Cochran et al., 1986; Zheng et al., 2002a; McManus et al., 2005; Morford et al., 2009b; Jokinen et al., 2020), the depth and intensity of the sulfate-methane transition zone (SMTZ) in the sediment (the term "intensity" refers to rate of sulfide production, including through organoclastic sulfate reduction and sulfate-mediated anaerobic oxidation of methane) (Jokinen et al., 2020), sedimentation rate (Algeo and Maynard, 2004; Scott and Lyons, 2012; Noordmann et al., 2015; Liu and Algeo, 2020), and local detrital (Al) background (van der Weijden, 2002; Brumsack, 2006). The magnitude of these caveats and the extent to which they impact sediment-based Mo- and U-enrichment factors (Mo-EFs, U-EFs) in different redox conditions and depositional environments are poorly constrained. Therefore, we investigate multiple sites across a range of depositional environments. With our comprehensive data set, we show that by using a combination of Mo and U enrichments, it is possible to deconvolve past redox conditions in coastal settings for which monitoring data are lacking.

2. Geochemical behavior of Mo and U

Molybdenum is present in seawater as dissolved molybdate (MoO_4^{2-}; Mo(VI); Bertine and Turekian, 1973) with an average concentration of 110 nM. Molybdate behaves conservatively and has an oceanic residence time of ~440 thousand years (Miller et al., 2011). Under oxygenated conditions, Mo(VI) has little affinity for other components in the water column, with the exception of iron (Fe)- and manganese (Mn) (oxy)(hydr)oxides to which Mo can adsorb (Bertine and Turekian, 1973). Fe- and Mn (oxy)(hydr)oxides can efficiently shuttle Mo from the water column to the sediment surface (Berrang and Grill, 1974; Algeo and Lyons, 2006; Sulu-Gambari et al., 2017; Wagner et al., 2017). MoO_4^{2-} is released back to the ambient (pore) water once Fe- and Mn (oxy)(hydr)oxides dissolve under reducing conditions. Depending on the ambient H_2S pore water concentration and availability of other host phases, MoO_4^{2-} can be (re)scavenged by a more refractory phase (Pilipchuk and Volkov, 1974; Helz et al., 1996; Algeo and Maynard, 2004; Helz and Vorlicek, 2019).

When approaching an aquatic H_2S (H_2S_{aq}) threshold value, i.e. "geochemical switch", of ca. 11 μM (25 °C, pH 8.3), MoO_4^{2-} is sequentially transformed into highly particle-reactive Mo-sulfide species such as thiomolybdate ($Mo^{VI}O_xS_4^{2-}{}_x$; x = 1–4, Helz et al., 1996; Erickson and Helz, 2000), Mo polysulfide ($Mo^{IV}O(S_4)S^{2-}$; Vorlicek et al., 2004), or an inorganic $FeMo^{VI}S_4$ phase. Aging transforms the latter into an inert $FeMo^{IV}S_2(S_2)$ phase, which limits any further scavenging of Mo_{diss} by leading to an asymptotic Mo_{diss} concentration in the water column or in the pore water (Vorlicek et al., 2018; Helz and Vorlicek, 2019; Helz, 2021). This process can explain lower sedimentary Mo enrichments in strongly euxinic basins compared to less euxinic basins (Helz, 2021).

In non-euxinic conditions, these mechanisms are limited to sedimentary sulfide fronts associated with high rates of organoclastic sulfate reduction (e.g., Rickard and Luther, 2007; Jørgensen et al., 2019;

Hermans et al., 2020) or sulfate-mediated anaerobic oxidation of methane (AOM, e.g., Boetius et al., 2000). Molybdate can also be released back from sediments into pore waters (and subsequently bottom waters) upon oxidation of labile host phases such as Fe monosulfide (FeS) and $FeMo^{IV}S_2(S_2)$ after re-oxygenation events (Sulu-Gambari et al., 2017; Hermans et al., 2019b; Dellwig et al., 2021).

Uranium is present in seawater as dissolved uranyl (UO_2^{2+}; U^{VI}) with an average seawater concentration of ~13 nM and a mean ocean residence time of 520 thousand years (Dunk et al., 2002). Under oxic conditions, uranyl commonly forms poorly-particle reactive uranyl-complexes, dominantly with carbonate ($UO_2(CO_3)_3^{4-}$; Garrels, 1955; Bonatti et al., 1971; Langmuir, 1978; Klinkhammer and Palmer, 1991). In contrast to Mo, authigenic U (U_{auth}) sequestered in sediments originates from diffusion across the sediment-water interface (SWI) regardless of the bottom water redox condition (Barnes and Cochran, 1991; Klinkhammer and Palmer, 1991; Algeo and Maynard, 2004; McManus et al., 2005), or from the deposition of Particulate Non-Lithogenic U (PNU) formed in surface waters, likely associated with particulate organic matter (Hirose and Sugimura, 1991; Zheng et al., 2002a). In sediments underlying an O_2 depleted water column, PNU can account for a substantial proportion of the total U_{auth} pool, whereas in sediments underlying oxic waters, the PNU fraction is negligible (Zheng et al., 2002a). Despite being seemingly unresponsive to shuttling by Fe- and Mn (oxy)(hydr)oxide in the water column, according to several laboratory experiments U, in its oxidized U^{VI} form, can be temporarily adsorbed to Fe- and Mn (oxy)(hydr)oxides in oxic surface environments (Brennecka et al., 2011; Singh et al., 2012; Dang et al., 2016). Permanent sequestration, however, requires reducing conditions to convert soluble and unreactive U^{VI} to insoluble and particle reactive uraninite (UO_2; U^{IV}; Veeh, 1967; Bonatti et al., 1971; Anderson et al., 1989; Klinkhammer and Palmer, 1991). Thermodynamics largely control U^{VI} reduction, but Fe and sulfate-reducing bacteria likely mediate the reduction process (Lovley et al., 1991, 1993; Zheng et al., 2002b; McManus et al., 2005; Bargar et al., 2013; Lee et al., 2014). In sediments, U present as refractory crystalline uraninite or labile monomeric "non-uraninite" U^{IV} typically binds to organic matter and organic carbon-coated clays (Bernier-Latmani et al., 2010; Bone et al., 2017). Owing to its labile mineral structure, monomeric U^{IV} is prone to oxidation by dissolved oxidants, such as O_2, or solids, such as Fe- and Mn (oxy)(hydr) oxides (Wang et al., 2013, and references therein) and re-mobilization as U^{VI} (Alessi et al., 2012) and subsequent upward diffusion to the overlying water column, or downward diffusion into the sediment (Cochran et al., 1986; Zheng et al., 2002a; Sundby et al., 2004; McManus et al., 2005; Morford et al., 2009a; Dellwig et al., 2021). These processes can limit the application of U as a redox proxy in sediments subject to bioturbation (Zheng et al., 2002b; Morford et al., 2009a), bioirrigation (Martin and Sayles, 1987), or (re)-oxygenated bottom waters (Cochran et al., 1986; Shaw et al., 1994; Zheng et al., 2002a).

3. Materials and methods

3.1. Study sites and data collection

In our investigation, we use solid-phase geochemical data of 18

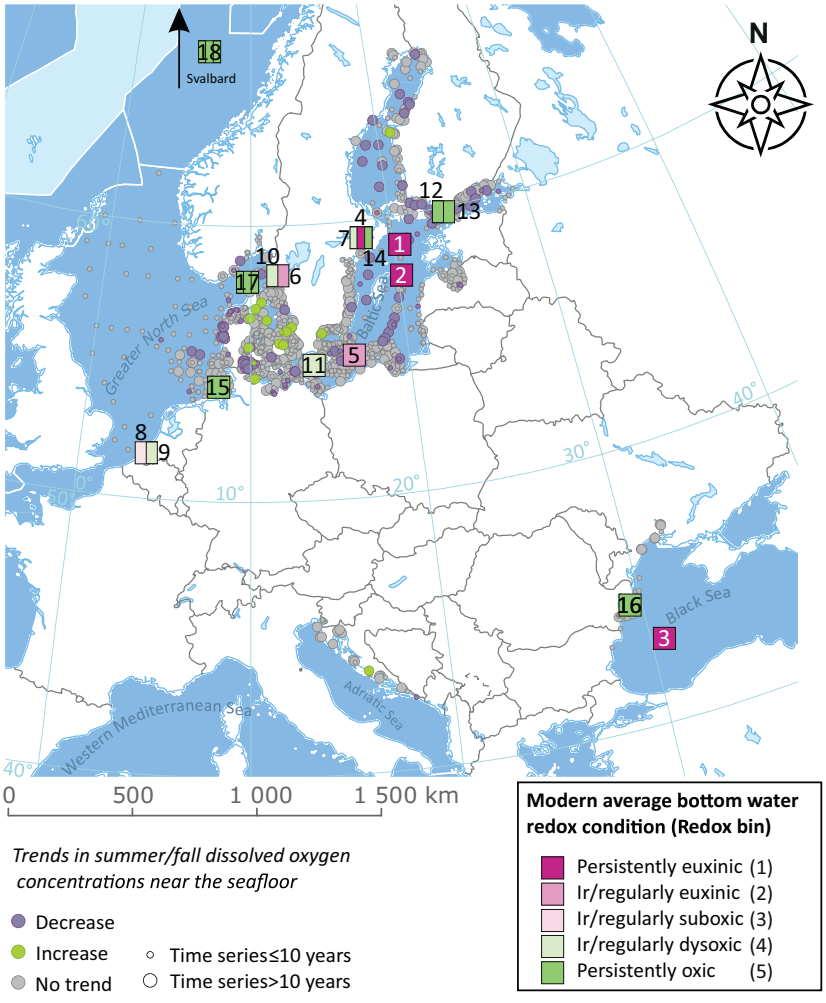

Fig. 1. The geographical location of the 18 study sites (filled squares) plotted together with the trends in summer/autumn dissolved O_2 concentration near the seafloor as determined by monitoring data (filled circles; European Environment Agency, EEA, 2019). The color of the squares corresponds to their modern average bottom water redox condition (redox bin, see legend at bottom right). Sites in close proximity are displayed as segmented squares. The number of segments corresponds to the number of sites. If the study sites have different redox bins, the segments have different colors. The location of the Svalbard sites is not captured by the map view. For coordinates, and geochemical and physical properties of the depositional environment of all study sites, we refer to Tables 2 and S1. Modified from EEA (2019).

coastal depositional environments in Europe (Fig. 1, Table 2). The study sites were selected based on covering a range of bottom water O_2 concentrations, as well as distinct differences in their depositional environments, including geographical location, bathymetry, sedimentation rate, degree of eutrophication, and salinity (Fig. 1, Tables 2, S1, and S2). For further analysis, the study locations were grouped into five "redox bins" according to ranges of bottom water O_2 conditions (Fig. 1, Table 2), broadly based on the redox classification by Algeo and Li (2020) for sedimentary environments (Table 1): persistently euxinic (redox bin 1), ir/regularly euxinic (redox bin 2), ir/regularly suboxic (redox bin 3), ir/regularly dysoxic (redox bin 4), and persistently oxic (redox bin 5). The term ir/regularly comprises locations with irregular or regular episodical (less than once per year), periodical (several times per year), or seasonal (each season) redox changes. The allocation of each site into redox bins was mainly based on available bottom water O_2 and hydrogen sulfide data (from either monitoring, or literature data). For details regarding monitoring data availability, temporal coverage, and monitoring frequency we refer to Table 2. The period of deposition used to allocate sites to a given redox bin varies from one location to another depending on the core length (full core solid-phase profiles were considered in this study; Fig. S1). At four sites, the sediment data series was divided into two segments with different redox bins, because of distinct temporal shifts in water column O_2 conditions during the period of sediment deposition (Table 2). This led to a double listing of four study sites, giving a total number of 22.

3.2. Solid-phase analyses

Methods of solid-phase analyses are summarized below. For detailed sampling procedures we refer to the source literature (Table S1, S2).

3.2.1. Sediment sampling

Sediments for solid-phase analyses were recovered with various coring devices (i.e., multicorer, UWITEC or GEMAX™) and sectioned at 0.4–5 cm intervals. Sediment samples were treated under O_2-free conditions (i.e., inside a N_2 or argon filled glove bag or box) to avoid oxidation of the samples. For further analyses (water and salt contents, porosity, total organic carbon (C_{org}) content, and total trace metal concentrations), sediment samples were (freeze)-dried, powdered, homogenized, weighed, and sub-sampled.

3.2.2. Determination of organic carbon content

The protocols for the determination of total C_{org} contents were comparable for all sites. The protocols included decalcification, drying and subsequent thermal combustion using a CNS analyzer. Samples from Koverhar and Lappohja were not decalcified, due to expected low carbonate contents (~1.1 wt%; Virtasalo et al., 2005; Jilbert et al., 2018; Jokinen et al., 2020). Data were checked against in-house standards and internationally certified analytical references (such as IVA2, sulfamethazine, or GPA 2186A). Organic carbon contents were corrected for weight loss upon decalcification and salt content of the freeze-dried sediment. The average analytical uncertainty (relative standard deviation, RSD %) based on duplicates was <3% for all samples. For analytical uncertainties in the published data, we refer to the original publications (Table S2).

3.2.3. Total elemental contents

The protocols for the determination of sedimentary major and trace metal concentrations (Al, Mo, and U) were comparable for all sites. Aliquots of (freeze)-dried and powdered sediment samples were digested using a triple-acid ($HClO_4$/HNO_3/HF) digestion protocol, redissolved in HNO_3 (Mort et al., 2010; Jilbert and Slomp, 2013b; Zhang et al., 2016; Kraal et al., 2017; van Helmond et al., 2018; Lenstra et al., 2019; Bennett and Canfield, 2020; Jokinen et al., 2020). The sample residues were analyzed by ICP-MS for Mo and U and/or ICP-OES for Al (and in some cases for Mo, e.g., for Lappohja pockmark and Den Osse St. 1, 8/2012). For analytical uncertainties of the elements in the published data, we refer to the original publications (Table 3). The accuracy (recovery) of all new data was based on in-house standards and commercial sediment reference materials (ISE-921, or MESS-4) and ranged between 91 and 106% (Mo), 89–109% (U), and 95–96% (Al), respectively. The precision (relative standard deviation, RSD %) based on sediment sample duplicates ranged between 3 and 5% (Mo), 2–5% (U), and 2–8% (Al), respectively. All elemental concentrations in the sediment were corrected for salt-dilution using the bottom water salinity and sediment porosity, assuming a solid-phase density of 2.65 g cm^{-3} (Burdige, 2006). For a small set of samples of three sites within redox bins 1, 4, and 5 ($n = 74$), the average recovery for Al was 127%. This was considered to reflect instrumental drift, and therefore a 27% correction factor was applied to all samples in the series in question. The corrected Al values were validated for Gullmar Fjord and Koljö Fjord samples by previous analysis of samples from the same study sites (September 2018, this study), and for German Bight samples from estimates of nearby study sites (Hinrichs, 2001).

3.2.4. Authigenic trace metal concentrations and enrichment factors

Many trace elements are also present in the detrital fraction of sediments (Wignall and Myers, 1988), thus, only trace metal enrichments corrected for their detrital fraction (= authigenic enrichments) can be used to reconstruct the redox state at the time of deposition and provide insights on the enrichment pathway. Three widely accepted methods are applied to estimate authigenic trace metal enrichments: TM/Al – ratio (e.g., Bennett and Canfield, 2020); TM-EF (e.g., Calvert and Pedersen, 1993; Tribovillard et al., 2004); and the excess trace metal content (TM_{XS}, e.g., Scholz et al., 2013; Jokinen et al., 2020). However, none of these methods is free of potential limitations (Reimann and De Caritat, 2000, 2005; van der Weijden, 2002; Brumsack, 2006; Cole et al., 2017). A strong criticism of the normalization methods centers on their use of "average shale" (Turekian and Wedepohl, 1961), Post-Archean Australian shale (PAAS, Taylor and McLennan, 1985, 1995), or upper continental crust (UCC, McLennan, 2001; Rudnick and Gao, 2014) as a substitute for local detrital background TM/Al values. For most elements enrichment factors are broadly similar between average shale, PAAS, and upper continental crust and average shale (Brumsack, 2006; Tribovillard et al., 2006; Tribovillard, 2020), implying that data from different studies using different reference material are comparable. Choosing a reference material that is close to local source material can decrease the error in the estimations. However, over- or underestimations of the true local detrital background can still occur, particularly if the composition of the detrital background has not been constant over time (Little et al., 2015; van der Weijden, 2002; Brumsack, 2006), or when it is low in Al (e.g. in carbonate rocks; van der Weijden, 2002). The use of true local background TM/Al content would be preferred over reference values. As these data were not available for our study sites, UCC values were used instead to objectively identify differences between a range of depositional redox environments with regards to their TM enrichments.

We chose the TM-EF as a primary trace metal redox proxy using UCC to increase the comparability with other studies. First, Mo and U contents were normalized against Al to distinguish the authigenic enrichment from the lithogenic background. Next, the sample ratios were divided by the average continental crust ratio of Mo/Al and U/Al to calculate the Mo and U enrichment factors (eq. 1).

$$TM - EF = \left(\frac{TM}{Al}\right)_{sample} \Big/ \left(\frac{TM}{Al}\right)_{reference} \quad (1)$$

where TM_{sample} is the measured Mo or U content, Al_{sample} is the measured Al content, and $TM/Al_{reference}$ represents the global UCC ratio for Mo and U against Al. Reference values (Al: 8.15 wt%, Mo: 1.1 ppm, and U: 2.7 ppm, Table S3) were taken from Rudnick and Gao (2014), because these represent the most recent and complete UCC composition

Table 2
List of study sites categorized in redox bins (1–5) based on their modern average bottom water redox condition, estimated based on monitoring data and literature. Physical and chemical bottom water (BW) data (temperature, salinity, O_2, H_2S) at the time of sampling is provided. BDL = Below Detection Limit. Further details about the study sites and monitoring data are provided in Table S1 and the listed references.

Study site	Water mass restriction	Water depth (m)	BW temp. (°C)	BW salinity (–)[f]	BW O_2 (μmol/L)	BW H_2S (μmol/L)	Reference	Approx. decade (redox bin[a])	Monitoring period (~monthly)	Reference
Modern average bottom water redox conditions (redox bin)[a]: Persistently euxinic (1)										
1. Fårö Deep[b] (F80)	Strong	191	6.6	12.0	*BDL*	45.6	Lenz et al. (2015)	~1960s	1963–2009	SMHI (2020), Carstensen et al. (2014)
2. Northern Gotland Basin[b] (LL19)	Strong	169	6.1	11.4	*BDL*	19.9	Lenz et al. (2015)	~1960s	1963–2009	SMHI (2020), Carstensen et al. (2014)
3. Black $Sea_{NW\ Abyssal\ plain}$ (St. 2)	Strong	2107	9.1	22.3	*BDL*	418	Dijkstra et al. (2018)	Based on basin wide residence time (>50 m of 387 yrs.; Murray et al., 1991)		
4. Skurusundet (St. 7)	Strong	27	2.8	5.3	*BDL*	10	This study	~1990s	1992–2017	SMHI (2020), site: Lännerstasundet
Ir/regularly euxinic (2)										
5. Bornholm Basin[b] (BY5)	Moderate	89	8.9	16.2	4		Lenz et al. (2015)	~1970s	1958–2007	SMHI (2020), Carstensen et al. (2014)
6. Koljö Fjord (KF-43 1–3)[c]	Moderate	43	5.1–6.7	27.7–29.1	*BDL*–138	*BDL*–27	This study	~1960s	1951–2018	SMHI (2020), Nordberg et al. (2001)
7. Lilla $Värtan_{pre\ 1990}$ (St. 5)	Moderate	21	2.3	4.9	55		This study	~until 1980s	1968–2017	SMHI (2020), site: Nyvarp
Ir/regularly suboxic(3)										
8. Den Osse $Basin_{deep}$ (St.1 8/2012; 3/2020)[c]	Strong	34	16.8, 6.9	32.1, ~ 31.7	3, 248	*BDL*	Hagens et al. (2015); This study	~late 1970s	1978–2020	Rijkswaterstaat (2020)
5. $Bornholm\ Basin_{pre\ 1970s}$[b]	Moderate	89	8.9	16.2	4		Lenz et al. (2015)	~until 1970s	1958–2007	SMHI (2020), Carstensen et al. (2014)
Ir/regularly dysoxic (4)										
1. $Fårö\ Deep_{pre\ 1970s}$[b]	Strong	191	6.6	12.0	*BDL*	45.6	Lenz et al. (2015)	~until 1970s	1950–2009	SMHI (2020), Carstensen et al. (2014)
2. $Northern\ Gotland\ Basin_{pre\ 1970s}$[b]	Strong	169	6.1	11.4	*BDL*	19.9	Lenz et al. (2015)	~until 1970s	1950–2009	SMHI (2020), Carstensen et al. (2014)
7. Lilla Värtan (St. 5)	Moderate	21	2.3	4.9	55		This study	~1980s	1968–2017	SMHI (2020), site: Karantänbojen
9. $Den\ Osse\ Basin_{slope}$ (St. 2 8/2012)	Strong	23	~17	32.2	12		Temperature based on S1 at 20 m water depth; Hagens et al. (2015)	~late 1970s	1978–2020	Rijkswaterstaat (2020)
10. Gullmar Fjord (GF-117 1–3)[c]	Moderate	117	6.6–7.1	34.4–34.5	71–219		This study, Brinkmann et al. (2021)	~1970s	1983–2019	SMHI (2020)
11. Arkona Basin (BY2 2007, 2009)[c]	Moderate	47	13, 15.6	12.2, 15.6	<2, 231		Mort et al. (2010), Jilbert et al. (2011)	~1960s	1985–2009	SMHI (2020)
Persistently oxic (5)										
12. Koverhar (St. 1–4)[d]	Mild	16–23	4.2–7.6	5.4–5.6	200–231		Jokinen et al. (2020)		1974–2019	Hertta (2021), sites: Tvärminne Storfjärden 106–110 + 152
13. $Lappohja_{inactive\ pockmark}$(E)	Mild	12	9.9	5.9	10		This study, hydrographical data from pockmark D (October 2019)		1974–2019	Hertta (2021), sites: Tvärminne Storfjärden 106–110 + 152
14. Sandöfjärden (St. 3)	Mild	64	2.1	5.8	150		This study		1968–2017	SMHI (2020), site: Nyvarp
15. German Bight (St. 6)	None	30	18.3	32.2	213		This study		1980–2010	Topcu and Brockmann (2015)
16. $Black\ Sea_{NWshelf}$ (St. 13)	Strong	13	9.2	18.1	209		Lenstra et al. (2019)		Dijkstra et al. (2018), Lenstra et al. (2019)	
17. $Skagerrak_{central\ eastern}$ (S4, 6, 9)[d]	None	190, 380, 695	6–7	35.0	230, 230, 260		Canfield et al. (1993)		Bennett and Canfield (2020)	
18. $Svalbard_{artic\ fjords}$ (SV2, 3, 5)[d, e]	Mild-none	115, 155, 175	2.6, 0.2, -1.7	34.7, 34.6, 34.9	321, 347, 328		Glud et al. (1998), Jørgensen et al. (2005)		Bennett and Canfield (2020)	

[a] Timescales for modern average bottom water redox conditions vary for each site, depending on available monitoring data.
[b] Fårö Deep, Northern Gotland Basin, Bornholm Basin, and Lilla Värtan were divided into two core sections with different redox bins, due to major changes in bottom water redox conditions during the period covered by the sediment core (Fig. S1). The timing of these changes was estimated based on monitoring data.
[c] Multiple campaigns from the same sampling sites with no significant redox bin variability were summarized as one data set.
[d] Data from the three sites were combined.
[e] Svalbard site SV1 (Bennett and Canfield, 2020) was excluded, because it is located in northern Norway and not on Svalbard.
[f] At time of sampling (Table S1).

Table 3
References for the sources of Mo and U data for all study sites.

Study site	References	
	Mo/Al	U/Al
1. Fårö Deep[a] (F80)	Jilbert and Slomp (2013a), van Helmond et al. (2018)	van Helmond et al. (2018)
2. Northern Gotland Basin[a] (LL19)	Jilbert and Slomp (2013a), van Helmond et al. (2018)	van Helmond et al. (2018)
3. Black $Sea_{NW\ Abyssal\ plain}$ (St. 2)	*This study*	*This study*
4. Skurusundet (St. 7)	*This study*	*This study*
5. Bornholm Basin[a] (BY5)	Mort et al. (2010)	*This study*
6. Koljö Fjord (KF-43 1–3)	*This study*	*This study*
7. Lilla Värtan (St. 5)[a]	*This study*	*This study*
8. Den $Osse\ Basin_{deep}$ (St.1 8/2012; 3/2020)	Sulu-Gambari et al. (2017), *This study*	*This study*
9. Den $Osse\ Basin_{slope}$ (St. 2 8/2012)	Sulu-Gambari et al. (2017)	*This study*
10. Gullmar Fjord (GF-117 1–3)	*This study*	*This study*
11. Arkona Basin (BY2 2007, 2009)[b]	Mort et al. (2010), *This study*	*This study*
12. Koverhar (St. 1–4)	Jokinen et al. (2020)	Jokinen et al. (2020)
13. $Lappohja_{inactive\ pockmark}$ (E)	*This study*	*This study*
14. Sandöfjärden (St. 3)	*This study*	*This study*
15. German Bight (St. 6)	*This study*	*This study*
16. $Black\ Sea_{NWshelf}$ (St. 13)	*This study*	*This study*
17. $Skagerrak_{central\ eastern}$ (S4, 6, 9)	Bennett and Canfield (2020)	Bennett and Canfield (2020)
18. $Svalbard_{artic\ fjords}$ (SV2, 3, 5)	Bennett and Canfield (2020)	Bennett and Canfield (2020)

[a] References refer to both core sections of Fårö Deep, Northern Gotland Basin, Bornholm Basin, and Lilla Värtan stated in Table 2.
[b] Only Mo data were available for the two campaigns.

estimates.

For comparison to alternative approaches such as sample TM/Al, and TM_{XS}, we additionally calculated the TM_{XS} of each sample (eq. 2) and provide both the raw data of Al, Mo, and U (Supplementary Material) and their concentrations in commonly used references materials (Table S3).

$$TMXS = TM_{sample} - \left((TM/Al)_{reference}\right) x\ Al_{sample} \quad (2)$$

where TM_{sample} is the trace metal content in the sediment sample, Al_{sample} is the Al content in the sediment sample, and $TM/Al_{reference}$ is the ratio between the trace metal and aluminum in a reference material. We followed the same approach as for the TM-EF calculation by using UCC background values.

3.2.5. Interpretation of TM-EFs

Commonly, TM-EFs are interpreted using arbitrary threshold values. An EF >1 indicates an enrichment relative to the crustal background, whereas an EF < 1 indicates a depletion (Tribovillard et al., 2004). Algeo and Tribovillard (2009) further differentiated between a detectable authigenic enrichment (EF > 3) and a substantial enrichment (EF > 10). In our study, we move away from arbitrary threshold values and instead look at the total ranges of the TM-EF at each site or within one redox bin. In each analysis, we used all data points from a given core (core lengths range between 0 and 50 cm) and considered the range of values using violin plots. We applied the same approach to sedimentary C_{org} contents, which are often considered alongside TM-EF data as an independent proxy for redox conditions (e.g., Bennett and Canfield, 2020).

We further test the use of combined Mo-EF vs. U-EF ratio data as a simple tool to assess controls on TM enrichment mechanisms (Algeo and Tribovillard, 2009; Tribovillard et al., 2012; van Helmond et al., 2018). Algeo and Tribovillard (2009) differentiated three key controls that impact on relative enrichments of the two elements: (A) benthic redox variations (average bottom water redox conditions and degree of variability; for the purpose of our study, we divided these into A1. and A2), (B) operation of a particulate Fe/Mn (oxy)(hydr)oxide "shuttle", and (C) changes in the water mass chemistry related to the degree of water mass restriction (Fig. 2). According to the conceptual model, minor bottom water redox variations (A1) are reflected first in U-EF, while a variation towards increased organic matter degradation and release of sulfide into the pore waters results in a coincident increase in both Mo-EF and U-EF, leading to a steepening of the gradient of Mo-EF vs. U-EF (A2). Controls B and C largely affect Mo-EF. The operation of a particulate "shuttle" (control B) can increase the transport of Mo from the water column to the SWI, favoring increased Mo-EF over U-EF even in mildly reducing systems. In strongly sulfidic and (semi)-restricted basins Mo sequestration may be limited by a combination of 1) insufficient hydrological resupply of Mo to the basin and simultaneous accelerated removal of Mo through the geochemical switch (the so-called "basin reservoir effect", Algeo, 2004, Algeo and Lyons, 2006), and 2) equilibrium of $FeMoS_4$ with Mo_{diss} at high sulfide concentrations (Helz, 2021). Both effects may result in a limitation of the maximum attainable Mo-EF, while U-EFs

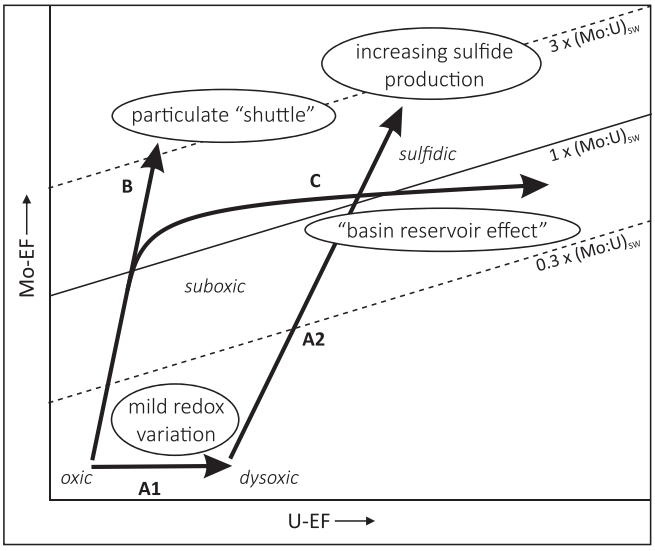

Fig. 2. Covariation patterns between Mo-EF and U-EF, modified from Algeo and Tribovillard (2009). The four black arrows and letters A1, A2., B, and C refer to the key enrichment controls: A1. and A2. bottom water redox variations (mild redox variations between oxic and dysoxic + increase in organic matter degradation and release of sulfide to the pore- and bottom waters), B operation of a particulate Fe/Mn (oxy)(hydr)oxide "shuttle", and C limited Mo sedimentary sequestration in sulfidic depositional environments (comprising the "basin reservoir effect" and equilibrium of $FeMoS_4$ with Mo_{diss} at high sulfide concentrations (Helz, 2021). Uranium is not affected by such mechanisms, and therefore continues to enrich in the sediment. The three diagonal lines represent multiples (0.3, 1, and 3) of the Mo:U ratio of present-day seawater (SW) converted to an average weight ratio of 3.1 for the purpose of comparison with sediment Mo:U weight ratios (Tribovillard et al., 2012).

continue to rise.

3.2.6. Statistics: Assessing variability and uncertainty in the dataset

Data variability and uncertainty between redox bin pairs, displayed as violin plots, were assessed based on both the spread of data using the Median Absolute Deviation (MAD, e.g., Pham-Gia and Hung, 2001), and 0.99 confidence intervals (CIs) of the mean using the bootstrapping resampling method (e.g., Carpenter and Bithell, 2000). Briefly, the narrower the range of the MAD and CI of the mean, the more reliable a generalized pattern can be deduced from the data. Both parameters were calculated in R (ggplot) using the stat_summary() function combined with the hmisc package. These methods were chosen, since the dataset is largely non-normally distributed and includes small subsample sizes (Rowland et al., 2021).

4. Results

4.1. Organic carbon contents

Sedimentary C_{org} contents are the highest among redox bin 1 sites (median: 8.2 wt%, Fig. 3A), and the lowest among redox bin 4 sites (median: 3.1 wt%). The smallest spreads (MAD) of C_{org} contents are observed for redox bins 2 and 3 (1.3 and 1.4 wt%), respectively. C_{org} ranges of redox bin 3 also have the highest certainty with a 0.99 CI of the mean of 0.5, compared to the largest uncertainty within redox bin 1 with a 0.99 CI of the mean of 1.4. The higher uncertainty in redox bin 1 coincides with a large data spread (MAD: 3.3 wt%), only the MAD of redox bin 5 is higher (3.4 wt%). Redox bins 1–3 show a considerable difference between each other (no overlap of the MADs), the differences between redox bins 3 and 5 are very weak, as the MADs show considerable overlap. Strikingly, instead of an expected decrease in C_{org} contents from bins 3 to 5 (increase in aerobic C_{org} degradation), C_{org} contents increase from redox bin 4 to 5 (medians: 3.1, 4.5 wt%), and are larger in redox bin 5 than in redox bin 3 (medians: 4.5 vs. 3.5 wt%). Given the inability to differentiate between redox bins 3–5, C_{org} contents alone do not accurately describe bottom water O_2 concentrations in our dataset.

4.2. Mo and U enrichment factors

4.2.1. Trace metal enrichments as a function of bottom water redox conditions

Sedimentary Mo-EF and U-EF patterns broadly resemble the C_{org} enrichment patterns, following the expected trend governed by bottom water redox changes (Fig. 3B and C). Highest EFs coincide with the most restricted and O_2 depleted sites of redox bin 1 (Mo-EF median: 103.7; U-EF median: 13.17), while lowest EFs coincide with the least restricted and O_2 depleted sites of redox bin 5 (Mo-EF median: 1.3; U-EF median: 1.8). However, each redox bin varies in the overall spread and CI of the mean for both EFs. The largest spread is observed for both EFs in redox bin 1 (Mo-EF MAD: 279.3; U-EF MAD: 29.0), coinciding with the largest 0.99 CI of the mean (Mo-EF: 46.3; U-EF: 6.02). In contrast, the smallest spread is observed in redox bin 5 (Mo-EF MAD: 1.9; U-EF: 0.9) with the highest certainty of 0.4 and 0.2 for Mo-EF and U-EF, expressed as 0.99 CIs of the mean. Overall, both the spread and confidence intervals are smaller across U-EF redox bins (MADs: 1.8–3.5; CIs: 0.2–0.4; excluding redox bin 1) than for Mo-EF redox bins (MADs: 1.3–38.4; CIs: 0.4–12.7; excluding redox bin 1).

The two elements show noticeable differences in their ability to reflect contrasts between the redox bins. Mo-EF resolves the contrasts between the more mildly reducing redox bins 3–5 (medians: 16.9, 3.2, 1.3), but the contrast is less strong between the more reducing redox bins 1–2, due to the overlap in the spread of the data of bins 1 and 2. Several samples of redox bin 4 and 5 sites plot below the average UCC background value (Mo/Al_{UCC}: 0.13 ppm/ wt%, horizontal dashed line, Fig. 3B). For U-EF, the strength of redox sensitivity is reverse to that of Mo-EF. While U-EF is very sensitive among redox bins 1–3 (medians: 13.2, 3.5, 1.8), between redox bins 3–5 no difference can be found, as the medians and MADs are within a similar range. Similar to Mo-EF, but

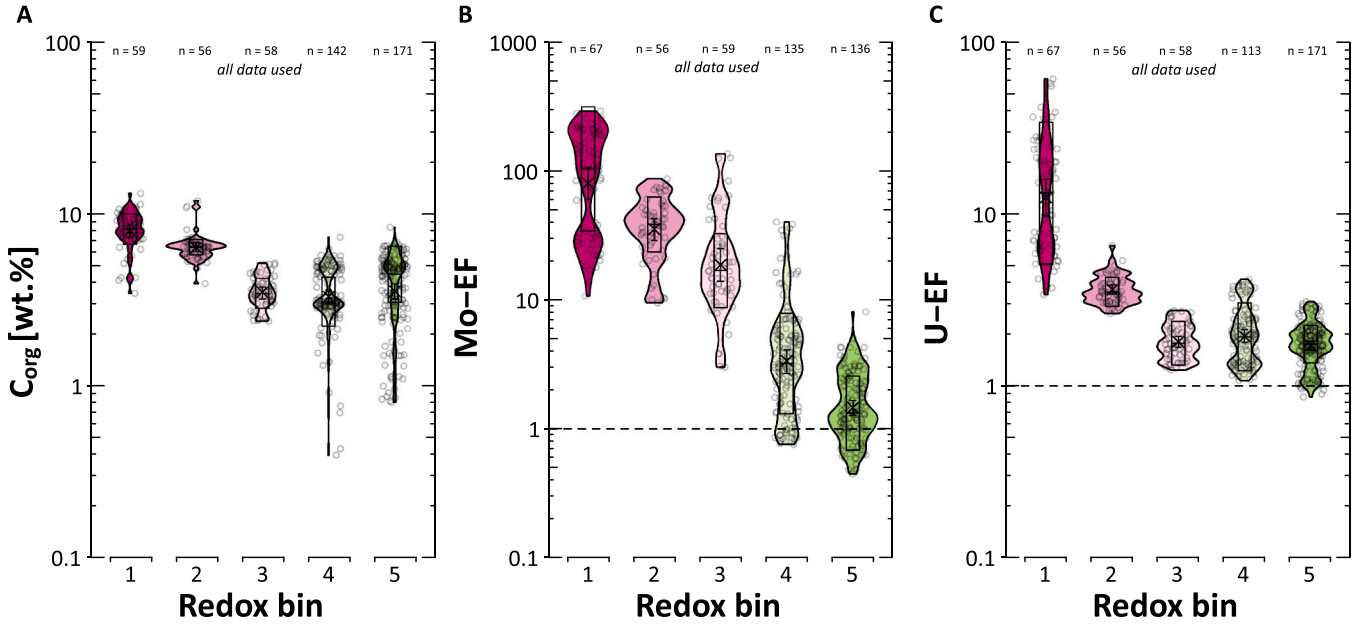

Fig. 3. A) Organic carbon content (wt%) for the different redox bins (Table 2) plotted as violin plots (log_{10} scale). Each violin plot represents the data distribution of each redox bin. The black cross and vertical black solid line with two whiskers within each violin plot denotes the mean with a 0.99 confidence interval (CI). The median absolute deviation (MAD) – a measure of the variability of non-normal distributed data – is illustrated by an empty vertical crossbar, divided by a horizontal black solid line, which represents the median. Numbering of the redox bins follows the scheme introduced in section 3.1: persistently euxinic (redox bin 1), ir/regularly euxinic (redox bin 2), ir/regularly suboxic (redox bin 3), ir/regularly dysoxic (redox bin 4), and persistently oxic (redox bin 5). B) Sedimentary Mo and C) U enrichment factors (EFs) across the redox bins (log_{10} scale). The horizontal dashed lines indicate the TM-EF value of 1, which is the threshold for authigenic Mo and U enrichments. Values below 1 indicate non-authigenic Mo and U concentrations. Data from organic-rich "fluffy" layers at the sediment surface of sites in redox bins 1–3 are not shown on this figure. Otherwise, all data points are shown. The total number of data points for each element and redox bin is given at top of each panel.

to a much lesser degree, selected samples from redox bin 5 sites have lower U_{auth} enrichments than the UCC background value (0.33 ppm/ wt %). In summary, both TM-EFs are stronger in reflecting bottom water redox changes than C_{org}. However, the large spread and confidence intervals across the redox bins indicate that additional controls likely play important roles in determining the magnitude of enrichment at any given location.

4.2.2. Station scale comparision of Mo- and U-EFs

To investigate the different sensitivity of Mo- and U-EF among the redox bins, all sites were plotted individually in order of decreasing mean Mo- and U-EFs. Broadly, the decreasing EFs correspond to changes in the redox bin classification of the sites from redox bin 1–5 (Fig. 4). Redox bin 1 sites have the highest EFs and redox bin 5 sites the lowest. However, there are several distinct anomalies in which the order of EF ranking deviates from that predicted by the redox bin, hence accounting for part of the observed overlap between the bins in the original analysis (Fig. 3B and C). We highlighted four examples of sites where either the Mo-EF or U-EF, or both, appear anomalous with respect to the redox bin classification (site numbers 4, 7, 8, and 10 in Fig. 4). Although this selection is partly arbitrary, since overlaps in TM-EFs between redox bins are reflected in multiple sites, the selection serves to illustrate key secondary factors influencing enrichments as described below. Site 4 has lower Mo-EFs compared to the other three sites of the same redox bin. The same observation is true for U-EF, although the difference is less distinct. Sites 7, 8, and 10 show a strong deviation from the expected U-EF ranking, but plot quite normally in Mo-EF. Additionally, we note that seven (Mo-EF) and two (U-EF) sites in redox bins 4 and 5 show data ranges that intercept with the average UCC background value; one such site has Mo-EFs considerably lower than the UCC (16. Black $Sea_{NW\ shelf}$). The anomalous patterns observed in the station-scale comparison confirm that additional site-specific controls beyond redox alone must affect the observed trace metal enrichments.

4.2.3. Mo- and U-EF covariation patterns

To assess the secondary factors controlling TM-EF, we begin by considering Mo-and U-EF covariation patterns according to the conceptual model of Algeo and Tribovillard (2009) (Figs. 2 and 5). For this approach, all sites were plotted individually to increase the interpretability. The results show that all three Mo- and U-EF covariation patterns in the conceptual model may be discerned in our study sites. Generally, redox bin 5 sites are only slightly enriched in Mo and U and show the characteristic steepening of the gradient of Mo-EF vs. U-EF above U-EF = 2 (Mo- and U-EF covariation patterns A1 and A2). Redox bin 4 sites are typically moderately enriched in Mo-EF, but a notable scatter is observed in Mo-EF vs. U-EF ratio, due to the variable effects of patterns A2 (increasing organic matter degradation and release of sulfide into the pore water) and B (activity of a particulate Fe/Mn (oxy)(hydr)oxide "shuttle") at different sites. Redox bin 3, which is represented by only two sites, plots at the higher end of the Mo-EF vs. U-EF gradient corresponding to covariation pattern B. Sites of redox bins 2 and 1 display the flattening of the Mo-EF vs. U-EF gradient corresponding to covariation pattern C, ceased Mo sequestration from sulfidic depositional environments, with redox bin 1 sites clustered towards the more extreme end of this gradient.

5. Discussion

5.1. Bottom water redox conditions as a primary control on Mo- and U-EFs

Both Mo-EF and U-EFs show contrasting behavior along the redox gradient, with Mo-EFs being a stronger proxy in mildly reducing depositional environments (redox bins 3–5), and U-EFs in stronger reducing depositional environments (redox bins 1–2). Nevertheless, both trace metals have in common that they show the largest enrichment at most reducing sites (redox bins 1 and 2, Fig. 3 B and C). This pattern is reproduced at the station scale (Fig. 4), with strongly reducing sites (redox bins 1 and 2) and mildly and non-reducing sites (redox bins 4 and 5) clearly differentiable. Therefore, we infer that the dominant control of Mo- and U-EFs at our coastal sites from a range of depositional environments is exerted by bottom water redox conditions. Our findings are thus in line with studies focusing on (strongly) restricted basins and continental margin OMZs in the modern ocean (McManus et al., 2005; Algeo and Lyons, 2006; van Helmond et al., 2018; Liu and Algeo, 2020; Bennett and Canfield, 2020).

In detail, however, our results demonstrate that both elements' EFs have considerable limitations in reflecting the whole range of small-scale redox variability (e.g., between redox bins 1 and 2, or 4 and 5). Mo-EFs show substantial differences between redox bins 3–5, but it is weaker in differentiating redox bins 1 and 2 (Figs. 3, 4, and 5). By contrast, U-EFs appear more suitable to detect variability between redox

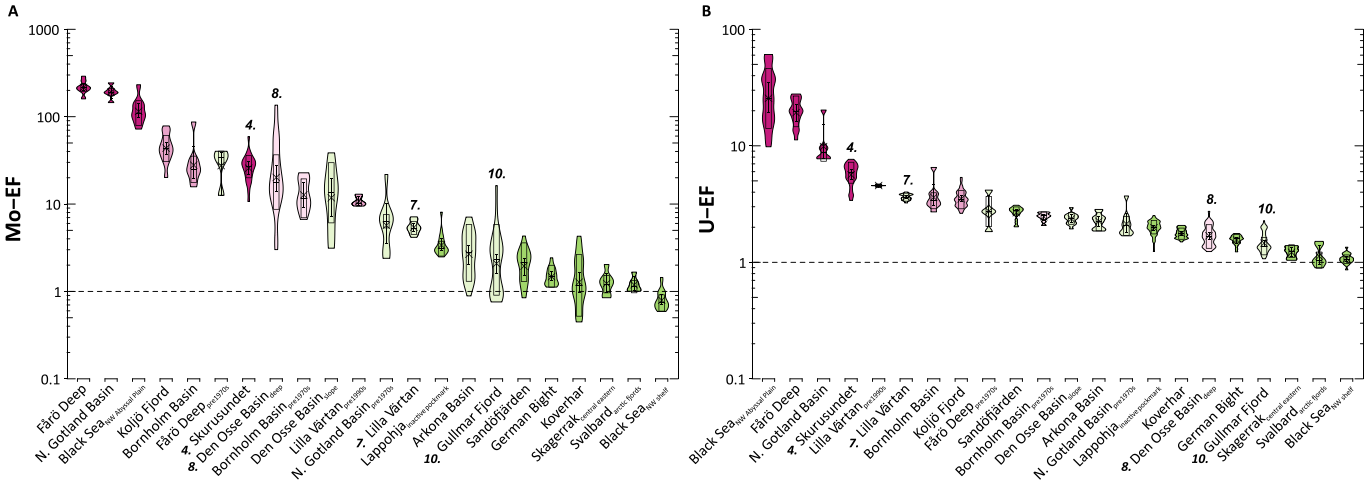

Fig. 4. Sedimentary A) Mo and B) U enrichment factors (EFs) among the study sites (log_{10} scale). For each element, the sites are arranged according to the order of their means, starting with the highest. The color of each box (site) corresponds with its redox bin (Fig. 3, Table 2). For some sites the total ranges vary between the two elements, due to different amounts of data points available (e.g., Lappohja, and Arkona, Table 2). Fårö Deep, Northern Gotland Basin, Bornholm Basin, and Lilla Värtan are listed twice: as the upper core section, covering the last <30–40 years, and as the lower core section, covering the preceding >30–40 years. The numbers refer to the sites that plot anomalously (see text). For detailed description of the violin plots see Fig. 3 caption). The horizontal dashed lines indicate the threshold for authigenic Mo or U enrichment (see Fig. 3 caption). Data from organic-rich "fluffy" layers are not shown on this figure.

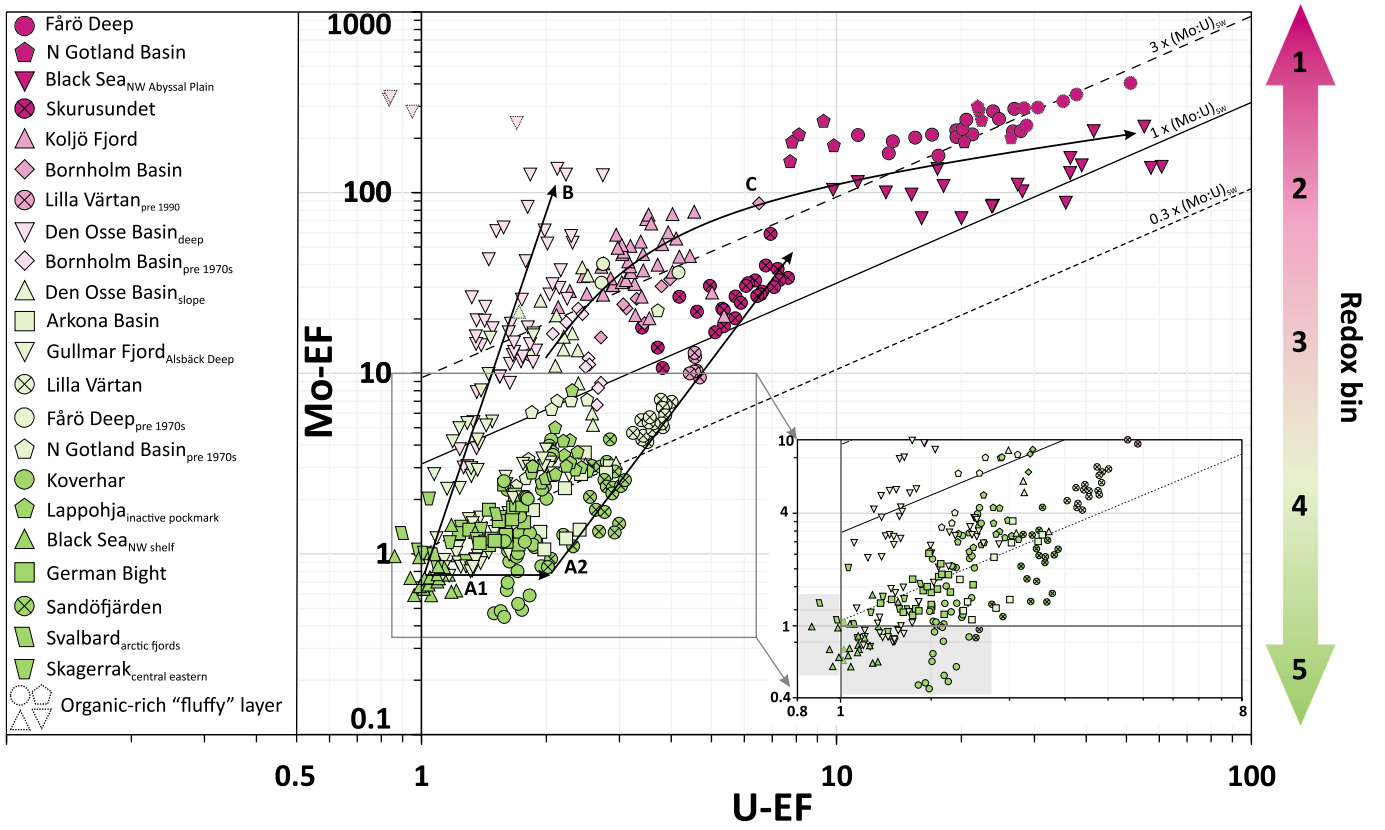

Fig. 5. Mo- and U-EF covariation patterns among the study sites based on whole core sediment samples (concept after Algeo and Tribovillard, 2009). The legend to the left shows all study sites with their corresponding bottom water redox color. The double arrow on the right shows the color coding of the redox bins 1–5 (Table 2). "Fluffy layer" samples are shown on this figure and indicated by dashed lines around the symbols. The two gray shaded boxes highlight the sites that have lower than UCC values for Mo and U. For detailed description of the lines and arrows, see Fig. 2 caption.

bins 1 and 2, but weaker in differentiating redox bins 4 and 5. The stronger differentiation potential of U-EF between redox bins 1 and 2 stands in contrast to a recent finding of Bennett and Canfield (2020), who found no evidence for U enrichment patterns that could reliably differentiate strongly reducing sites from less-reducing ones. A simple explanation for this deviation could be that these authors compared two very distinct types of depositional environments within the two redox bins (enclosed euxinic basins and open continental margin OMZs), while our sites are typically more comparable to each other with regards to their bathymetry within the same two redox bins. More striking, however, is the weaker differentiation potential of U compared to Mo between redox bins 4–5 because it stands in contrast to what is known based on their geochemical behavior. Based on existing knowledge, Mo should more reliable than U as redox proxy under (strongly) reducing bottom water redox conditions, due to the presence of hydrogen sulfide (e.g., Helz et al., 1996; Zheng et al., 2000), while U should be more sensitive than Mo under mildly reducing bottom water redox conditions, because U reduction occurs at higher reduction-oxidation potentials, likely governed by microbial activity (e.g., Zheng et al., 2002b; Lovley et al., 1991, 1993). Our contrasting findings suggest that certain site-specific or element-specific secondary factors are obscuring the initial redox signal. In this context, it should be reemphasized that C_{org} (Fig. 3A) shows a similarly striking (reverse) enrichment pattern to that of U-EF (Fig. 3B), which might suggest that U and C_{org} are affected by (a) similar factor(s) or they are directly, or indirectly, linked in their enrichment pathway. Next, a selection of possible site-specific or element-specific secondary factors will be discussed.

5.2. *Depositional environmental factors as secondary controls of Mo- and U-EFs*

Anomalies to the expected trends with variable redox conditions are a relatively common observation in sedimentary trace metal studies (Scott and Lyons, 2012; Bennett and Canfield, 2020). However, past studies that have investigated such anomalies have typically focused on a narrow selection of factors, namely depositional environments, and redox conditions (e.g., Algeo and Tribovillard, 2009; Liu and Algeo, 2020). Here, we systematically test the influence of six secondary factors controlling Mo- and U-EFs, while also considering the whole range of redox conditions and depositional environments. We identified four sites that have Mo-EF and/or U-EFs anomalous to their assigned redox bin (Fig. 4, station numbers 4, 7, 8, and 10), either by showing over- or under-enrichment. Below we discuss how depositional environmental factors can potentially bias either the Mo-EF, U-EF, or both.

5.2.1. *Limited Mo sequestration in sulfidic depositional environments*

Limited Mo sequestration in sulfidic depositional environments (pattern C, Fig. 5) can be explained by two processes. Once conditions become sulfidic, Mo sequestration may be limited by insufficient hydrological re-supply of Mo to the basin (the so-called "basin reservoir effect", Algeo, 2004, Algeo and Lyons, 2006). Alternatively, precipitation of Mo may be limited by the equilibrium of $FeMoS_4$ with Mo_{diss} at high sulfide concentrations (Helz, 2021). In contrast, authigenic U enrichment under sulfidic redox conditions is not determined by such solubility effects, but rather by the activity of iron and sulfate reducing bacteria (Lovley et al., 1991, 1993). Uranium also shows generally lower sensitivity to the basin reservoir effect (Algeo and Maynard, 2008; Tribovillard et al., 2012; van Helmond et al., 2018). We interpret pattern

"C" of the Mo-EF vs. U-EF covariation patterns (Fig. 2) to indicate a combination of the above effects, whereby the enrichment of Mo is limited with respect to U in the most sulfidic settings (Fig. 5). Sites that show this enrichment pattern are typically subject to severe deoxygenation in response to strong water mass stratification, and restricted water mass exchange, which gradually depletes the pool of sequesterable Mo (Algeo and Lyons, 2006; Tribovillard et al., 2006; van Helmond et al., 2018). Three of the four sites in redox bin 1 show a clear signal of such effects with limited Mo enrichment in comparison to U (Fig. 5). Using is cross-plots of unnormalized sedimentary Mo, and C_{org} enrichments (as per Algeo and Lyons, 2006; Algeo and Rowe, 2012; Tribovillard et al., 2012; van Helmond et al., 2018), we show that all four sites in redox bin 1 show signs of a considerable sedimentary Mo depletion relative to C_{org} (Fig. S7A). Notably, the anomalous site 4. Skurusundet (Fig. S7A) shows the lowest Mo/C_{org} of any location in the dataset, implying the strongest sedimentary Mo depletion of the redox bin 1 sites. Based on our knowledge, this may be the first described shallow, low salinity (Table 2), and strongly euxinic depositional environment for which limitation effects on Mo sequestration have been identified. Moreover, we postulate that the anomalously low U enrichments at the same site could be explained by water column depletion of U_{diss} (i.e. basin reservoir effect), a phenomenon previously described for the strongly euxinic Kyllaren Fjord, Norway (Noordmann et al., 2015).

5.2.2. The particulate Fe and Mn (oxy)(hydr)oxide shuttle

The particulate Fe and Mn (oxy)(hydr)oxide shuttle (pattern B, Fig. 5) can enhance the rate of sequestration of Mo to sediments due to sorption of Mo_{diss} onto particle surfaces (Algeo and Tribovillard, 2009; Jilbert and Slomp, 2013b; Scholz et al., 2014; Sulu-Gambari et al., 2017; Lenstra et al., 2019). Once Fe and Mn (oxy)(hydr)oxides are dissolved below the oxic-suboxic redox boundary, Mo is released to the pore water or water column. Depending on the availability of more refractory host phases, Mo_{diss} is either (re)sequestered, e.g., by FeS, or diffuses upward to overlying oxic water. The efficiency of this shuttle mechanism is dependent on the amount of Fe and Mn input from the water column or through remobilization by bioturbation, bioirrigation, or pore water acidification by cable bacteria (Seitaj et al., 2015; Sulu-Gambari et al., 2016; Hermans et al., 2019a; Lenstra et al., 2019), and the vertical distance between Fe and Mn (oxy)(hydr)oxide formation and reductive dissolution (Sulu-Gambari et al., 2017). Although Fe- and Mn (oxy)(hydr)oxides can temporarily sequester U under oxic conditions in the solid phase, they do not play an essential role in the particle transport of U or serve as long term host phases for U (Morford et al., 2005; Wang et al., 2013; Jokinen et al., 2020). Therefore, in principle, active particulate shuttling will result in a high ratio of Mo-EF to U-EF (Fig. 2). Of our sites, this pattern can be identified for 8. Den Osse $basin_{deep}$ and 10. Gullmar Fjord (Fig. 5). These sites are from different redox bins, but are both seasonally stratified (Filipsson and Nordberg, 2004; Hagens et al., 2015), and show evidence for strong Mn oxide re-cycling in the water column, potentially enhancing sequestration of Mo (Sulu-Gambari et al., 2017; Goldberg et al., 2012). This typical enrichment pattern can explain why 8. Den Osse $Basin_{deep}$ shows anomalously low U-EFs and high Mo-EFs in the station-scale comparison (8, Fig. 4). Despite elevated Mo-EFs with respect to U-EFs, this pattern is less clear for 10. Gullmar Fjord because both elements' EFs are close to UCC values (Fig. 4). Generally, our results show that the Mo-EF and U-EF covariation model developed by Algeo and Tribovillard (2009) is applicable to identify the operation of the particulate shuttle at coastal sites. With respect to 10. Gullmar Fjord, seemingly, at least one other depositional environmental factor must be influencing Mo_{auth} and U_{auth} sequestration, which requires further investigation.

5.2.3. The depth and intensity of the SMTZ in the sediment

The combination of low-salinity (low sulfate concentration) and high labile organic matter loading in response to anthropogenic eutrophication (Fleming-Lehtinen et al., 2015) have led to an upwards migration of the SMTZ during the late 20th century to the uppermost 10–20 cm in many coastal areas of the northern Baltic Sea (e.g., Bothnian Sea and Gulf of Finland) (Slomp et al., 2013; Jilbert et al., 2018; Myllykangas et al., 2020). In such systems, a shallow and compacted SMTZ may catalyze the uptake of Mo and U even under oxic bottom water conditions, which may impact their applicability as redox proxies. To investigate the potential impact of the depth and intensity of the SMTZ depth as a secondary factor controlling Mo- and U-EFs, we propose the use of the ratio between C_{org} (C) and salinity (Sal), C/Sal hereafter. The approach is based on the reasoning that the depth of the SMTZ is largely controlled by the loading of labile organic matter (Slomp et al., 2013; Egger et al., 2015) and the ambient salinity, which controls the sulfate concentration (Jilbert et al., 2018). Since C_{org} and bottom water salinity are more routinely measured in sediment studies than porewater sulfide and methane profiles, C/Sal provides a useful proxy to estimate relative SMTZ depth between sites. Using the C/Sal value of the 12. Koverhar site (redox bin 5) as a reference, due to its known shallow SMTZ (Fig. 6, upper row; Jokinen et al., 2020), we tested whether sites with anomalous enrichments may be influenced by contrasting depths of the SMTZ. The redox bin 4 sites 7. Lilla Värtan and 10. Gullmar Fjord (Fig. 4) appear to fit this description; 7. Lilla Värtan U-EFs are anomalously high, while 10. Gullmar Fjord U-EFs are anomalously low, and their position in the U-EF range corresponds well with their C/Sal ratios. 7. Lilla Värtan has a high C/Sal ratio – correlating well with its shallow SMTZ (Dalcin Martins et al., 2022) – which could explain higher U-EFs compared to other redox bin 4 sites in response to increased authigenic sequestration of U within the sulfide front. By contrast, 10. Gullmar Fjord has a very low C/Sal ratio – indicating a deep SMTZ – yielding exceptionally low Mo-EF and U-EF for a redox bin 4 site, likely due to minimal sulfate reduction in the upper sediment column (Goldberg et al., 2012).

Besides the ability to explain anomalously high or low EFs, the C/Sal ratio may also help to explain the remaining uncertainty in the lower sensitivity of U-EF between redox bins 3–5. Three sites of the redox bin 5 sites (Koverhar, $Lappohja_{inactive\ pockmark}$, and Sandöfjärden) have C/Sal ratios indicating a shallow SMTZ, which is agreement with previous studies (Jokinen et al., 2020; Dalcin Martins et al., 2022). In addition, the sites have the highest Mo- and U-EFs among the oxic sites (Fig. 4). Through removing these three sites from our original data set, we were able to improve the sensitivity of U and Mo in the lower redox range considerably (Fig. 7C and B), compared to the original Fig. 3. This finding illustrates that enhanced Mo_{auth} and U_{auth} sequestration above the background are not restricted to low bottom water redox conditions, but can also be indicative of eutrophied, but oxic coastal depositional environments. Our approach had a similarly positive effect for C_{org}, in that the initial trend of increasing C_{org} contents from redox bins 3–5 was reversed and now is in line with the expected trend of decreasing C_{org} preservation at rising O_2 concentration (Fig. 7A). Consequently, the combination of a short water column, low salinity, high organic matter input, and high sedimentation rates – all common characteristics of a near coastal depositional environment (as present in the Baltic Sea) – is likely the cause of the high C_{org} contents at sites with oxygenated water columns, which sufficiently explains the higher C_{org} contents in redox bin 5 than in redox bins 3 and 4 (Fig. 3A).

5.2.4. Post-depositional remobilization

The impact of post-depositional remobilization of labile Mo and U mineral phases on the interpretation of sedimentary Mo-EF and U-EF is currently unknown. Generally, Mo can easily be remobilized upon reductive dissolution of labile Fe/Mn (oxy)(hydr)oxides (Sulu-Gambari et al., 2017; Dellwig et al., 2021), and oxidative dissolution of labile Mo-Fe-S phases (Hermans et al., 2019b). Consequently, Mo might escape into the water column, if redox conditions are insufficient (low sulfide levels) to fixate Mo at the surface sediments (Erickson and Helz, 2000). However, oxidative dissolution of refractory authigenic Mo phases (e.g., $FeMoS_4$) under natural conditions is highly unlikely due to irreversible

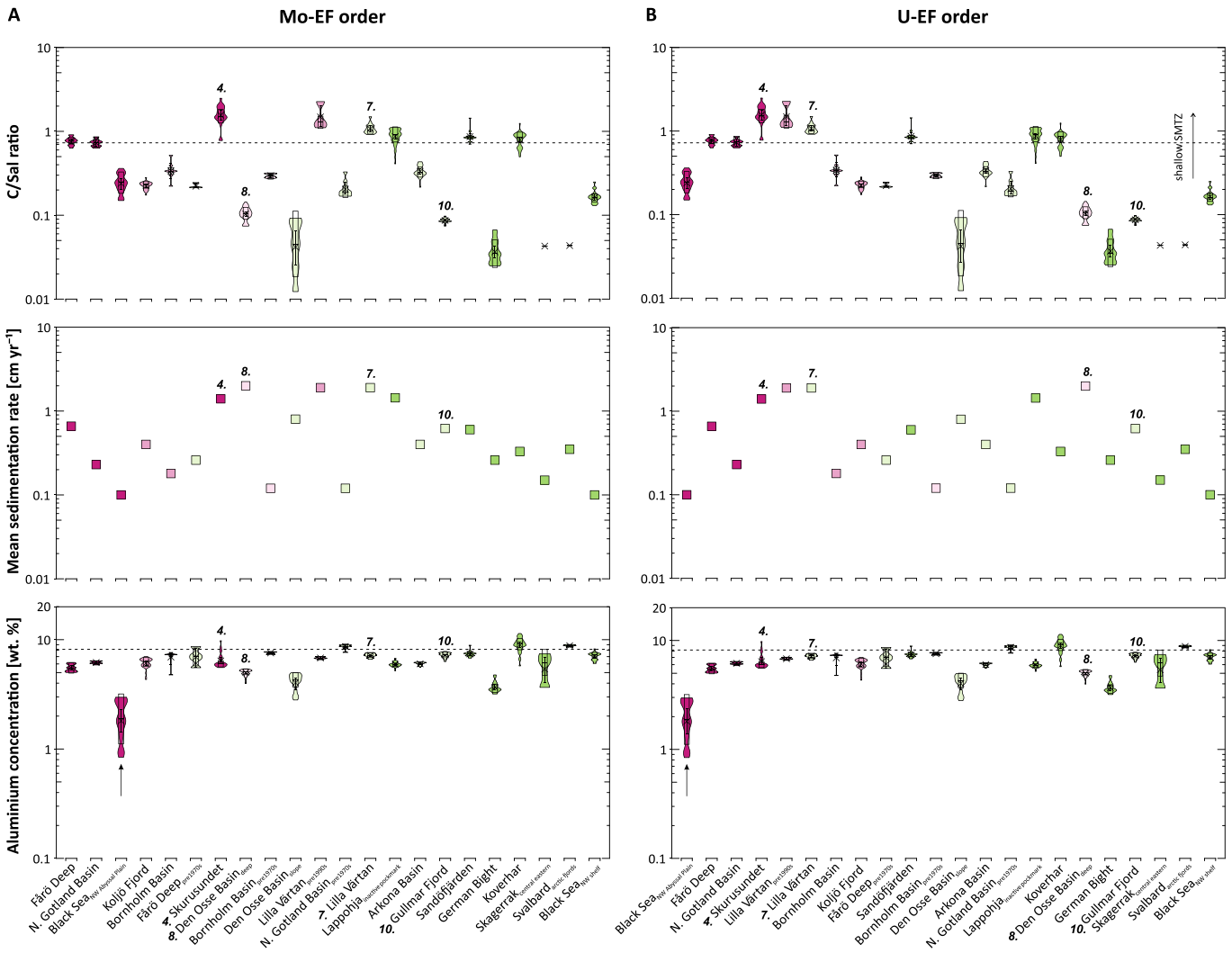

Fig. 6. Selection of three depositional environmental factors and their impact on A) Mo-EFs and B) U-EFs among the study sites (log_{10} scale). Upper row: C_{org}/salinity (C/Sal) ratio. The horizontal dashed line denotes the average C/Sal ratio at the reference site 12. Koverhar. The numbers represent the "anomalous sites" (see Fig. 4 caption). Middle row: whole core or core segment average sedimentation rates. Bottom row: whole core or segment Al concentrations (wt%). The arrow highlights the outlier site 3. Black $Sea_{NW\ Abyssal\ Plain}$. The horizontal dashed line indicates the Al_{UCC} value (8.15, Rudnick and Gao (2014). "Fluffy layer" data are not shown. For absolute values, and references see Table S2.

mineral formation kinetics (Erickson and Helz, 2000; Vorlicek et al., 2018; Jokinen et al., 2020; Helz, 2021). Similarly, post-depositional remobilization of U is dependent on the type of authigenic U species. Principally, the sedimentary U pool is thought to consist of a mixture of refractory uraninite and labile monomeric non-uraninite U^{IV} species strongly associated with organic matter (Bernier-Latmani et al., 2010; Sharp et al., 2011; Bone et al., 2017). Non-uraninite U^{IV} can easily be oxidized due to weak U—U bonds (Alessi et al., 2012). Therefore, study sites subject to sediment re-oxygenation in response to inflow events (Cochran et al., 1986; Shaw et al., 1994; Zheng et al., 2002a), bioturbation (Zheng et al., 2002b; Morford et al., 2009a), or bioirrigation (Martin and Sayles, 1987) could have lower Mo- and U-EFs than expected. These criteria theoretically apply to redox bins 2–5, although benthic macrofaunal activity is highly unlikely for redox bin 2 sites. For sites rates of high Fe/Mn (oxy)(hydr)oxide refluxing (8. + 9.: Den Osse Basin, and 10. Gullmar Fjord), we expect that any effluxed $Mo_{diss,}$ is efficiently returned to the sediments after trapping by oxides in the water column. Since both Den Osse Basin sites (8.: redox bin 3; 9.: redox bin 4) have Mo-EFs >10, this scenario is indeed likely. In contrast, U-EFs at these sites appear to be depressed, suggesting loss by re-oxidation. Redox bin 5 sites are most prone to post-depositional remobilization due to oxygenated bottom waters, and generally higher macrofaunal densities (e.g., Hermans et al., 2019a). However, among these sites we found a moderate to large scatter in U-EFs (1–3) and particularly Mo-EFs (⟨1−10), respectively. Generally, this speaks for sufficient Mo_{auth} and U_{auth} preservation for the vast majority of redox bin 5 sites, even if post-depositional re-mobilization occurs. Targeted site-specific studies are required to determine the actual impact of post-depositional re-mobilization for Mo- and U-EF at each site.

5.2.5. *Detrital dilution*

Detrital dilution of sedimentary Mo_{auth} and U_{auth} signals through high sedimentation rates has repeatedly been suggested as a critical factor for the applicability of Mo-and U-based redox proxies (Lyons and Kashgarian, 2005; Scott and Lyons, 2012; Noordmann et al., 2015; Liu and Algeo, 2020). Dilution effects caused by high sedimentation rates are suggested to lead to lower authigenic enrichments of both U (Anderson and Fleisher, 1991) and Mo (Lyons and Kashgarian, 2005). If true, this implies an inverse relationship between sedimentation rate and Mo- and U-EF values for sites with similar redox conditions. However, we found no clear evidence for such relationships in our data (Fig. 6, middle row). The sites within each redox bin show no systematic

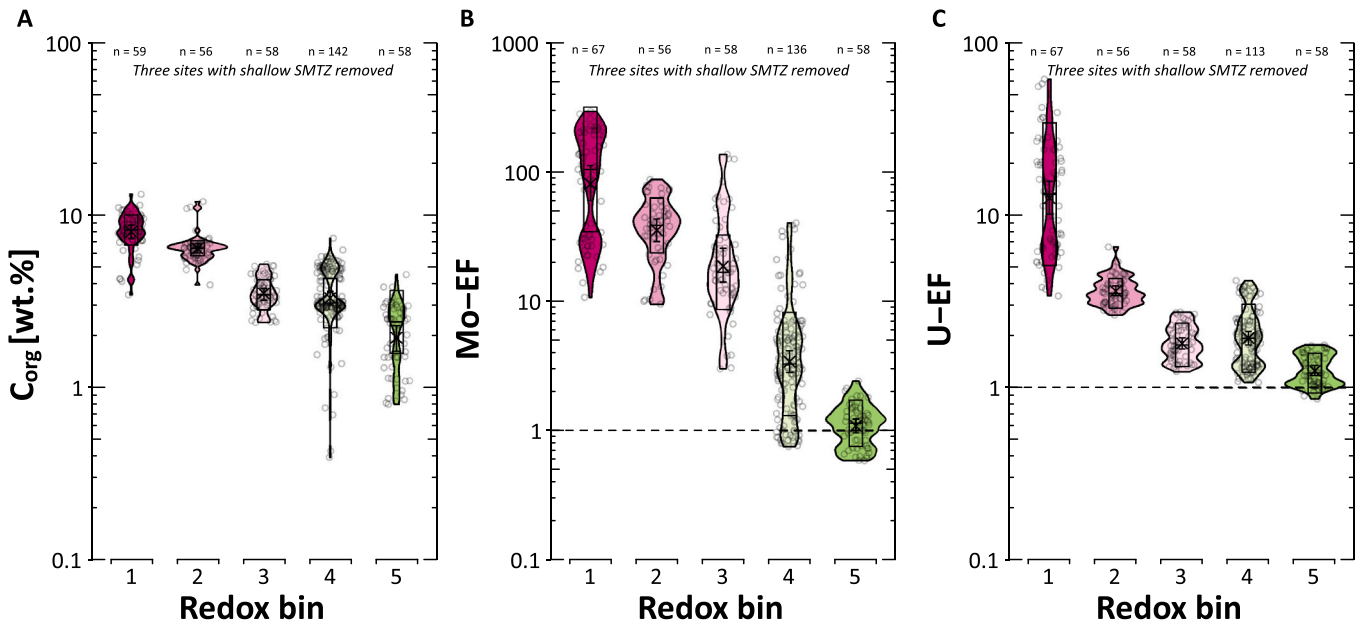

Fig. 7. Modified version of Fig. 3 to illustrate the impact of oxic sites with a shallow SMTZ (high C/Sal ratio) on the applicability of A) C_{org}, and B) Mo-EFs, and C) U-EFs. After the removal of sites Koverhar, Lappohja$_{inactive\ pockmark}$, and Sandöfjärden (see text for details), the differences between redox bins 4 and 5 have become more distinct, in particularly for U-EF (cf. Fig. 3). See Fig. 3 caption for details.

ordering towards lower EFs for higher sedimentation rate sites, implying that such effects, if present, are generally obscured by other variability. We note that sedimentation rates among our study sites range between ~0.1 cm yr^{-1} in the Black Sea (Wijsman et al., 2002; Lenstra et al., 2019) and ~ 2 cm yr^{-1} in the Den Osse Basin$_{deep}$ (Malkin et al., 2014). This range is considerably higher than the euxinic Black Sea sites with "high" (ca. 0.1 cm yr^{-1}) and "fairly high" (0.01 cm yr^{-1}) values reported in previous studies into the impact of sedimentation rates on TM-EFs (Algeo and Lyons, 2006; Scott and Lyons, 2012) and thus the conclusions of these studies may not be directly applicable to our data.

5.2.6. *Detrital Al background content*

The absolute TM-EF can be influenced by site specific detrital Al contents in such a way that a lower Al background content will lead to unrealistically high authigenic enrichments, or vice versa (Brumsack, 2006). To detect whether there are sites within this study showing considerably deviating local Al enrichments than the UCC$_{Al}$ background and thereby causing anomalous TM-EFs, we arranged the local sedimentary Al contents in the order of the Mo- and U-EFs (Fig. 6, lower row). Most sites have an offset to the UCC$_{Al}$ value of 10–30%. Five sites have an offset of >30%, of which one (3. Black Sea$_{NW\ Abyssal\ plain}$) has a 400% offset (black arrow, Fig. 6, lower row). This is the deepest of all studied sites (> 2000 m) and farthest from shore. Sediments in the pelagic Black Sea are typically starved of detrital material (low Al contents) and enriched in calcium carbonate (Pilipchuk and Volkov, 1974; Kraal et al., 2017), which likely yield an overestimation of the EFs (Little et al., 2015; Bura-Nakić et al., 2020). In the context of redox-sensitive trace metal studies, pelagic Black Sea sediments have commonly been normalized against global background values of PAAS or UCC (Algeo and Tribovillard, 2009; Algeo and Li, 2020; Yano et al., 2020), likely due to the lack of local background estimates, limited data availability of Al, Mo, and U contents in carbonates (Turekian and Wedepohl, 1961), and improved comparability with previous studies. Despite this discrepancy, since the majority of sites only show minor deviation from the UCC$_{Al}$ background, we infer that the effect of over- or underestimation, due to varying Al contents, is negligible among our study sites.

5.3. *Implications for the use of Mo- and U-EFs to reconstruct redox conditions in coastal depositional environments*

5.3.1. *Secondary depositional environmental factors*

Our results show that both Mo- and U-EF have limitations compromising their universal use as recorders of bottom water redox changes. These limitations are clearly linked to the influence of secondary

Table 4
A selection of depositional environmental factors impacting sedimentary Mo- and U-EF. Their impact power is indicated by symbols: -- strong negative impact (considerably lower enrichments than expected); ++ strong positive impact (considerably higher enrichments than expected); – negative impact (lower enrichments); + positive impact (higher enrichments); o no/ undetectable impact; +/– negative or positive impact (under–/overestimation); ? indication of impact power, but with uncertainty.

Depositional environmental factors	Mo-EF	U-EF	Reference
Limited sequestration under sulfidic conditions	--	–?	*This study*; Algeo and Tribovillard (2009); Tribovillard et al. (2012); Scholz et al. (2013); van Helmond et al. (2018)
Fe/Mn (oxy)(hydr)oxide"shuttle"	++	o	*This study*; Algeo and Tribovillard (2009); Tribovillard et al. (2012); Scholz et al. (2013)
Post-depositional mobilization (re-oxygenation)	o/–?	o/ –?	*This study*
Depth of SMTZ in the sediment (C/Sal)	+	++	*This study*; Jokinen et al. (2020)
Sedimentation rate	o/+?	o/ –?	*This study*
Local detrital (Al) background	+/–	+/–	*This study*

depositional environmental factors. When applying Mo- and U-EFs to reconstruct redox variability in a new study location, it may be challenging to identify each of the specific depositional environmental factors, assess the degree to which they impact Mo- and U-EFs, and finally, to correct for their influence on the data. Some depositional environmental factors can be easily identified (e.g., those reflected in the Mo- and U-EF covariation model established by Algeo and Tribovillard, 2009). As a result of the large heterogeneity among depositional environments, determination of most secondary factors requires additional data collection and analysis, such as water column trace metal concentrations, elemental mass accumulation rates, sediment grain size distributions, bioturbation and bioirrigation potentials, diffusive fluxes, and sediment trace metal speciation. A summary of potential depositional environmental factors that could impact Mo-and U-EFs is given in Table 4. This is intended as a guide to the careful interpretation of data from new study locations in coastal depositional environments.

Based on our data, we suggest that Mo is a more reliable redox proxy within redox bins 3–5 compared to U, likely because of a stronger sequestration potential in the sediment, particularly when H_2S is present in the pore water, and a lower oxidative dissolution potential. In contrast, we attribute the stronger reliability of U within redox bins 1 and 2 to the relative immunity of U to the processes limiting Mo sequestration in euxinic basins.

5.3.2. Data quality and definition of redox bins

A potential limitation to our approach is that the interpretations depend on the quality of the monitoring data used to assign the sites to a given redox bin. Although many of these sites have been intensively monitored for dissolved O_2 concentrations, the frequency of sampling, length of data series and maximum depth of water sampling are variable (Table 2). We use whole sediment core profiles with a range of temporal coverage that does not necessarily match that of the monitoring data when assessing the Mo-EF and U-EF ranges of each site (Fig. 1). It should also be noted that the sediment profiles show site- and element-specific differences and fluctuations in the Mo and U enrichments over time. These fluctuations can be indicative of either periodic variability in the bottom water redox conditions or of secondary depositional environmental factors as described above. A further concern in dynamic coastal settings is that a significant fraction of sedimentary material can be deposited from lateral transport (e.g., Jokinen et al., 2015), thus potentially obscuring the primary signal of redox conditions recorded in Mo- and U-EFs. Further investigations, such as assessment of grain size distributions combined with trace metal speciation may help to disentangle the reasons for within-site variability and to improve the understanding of Mo and U sequestrations in heterogeneous coastal sediments.

The approach of allocating sites to redox bins is also not free of limitation. In our dataset, each redox bin contains at least three different depositional environments with regards to bottom water salinity, temperature, sedimentation rate, and water depth (except for redox bin 3, which contains two sites, dominated by one site consisting of data from two different sampling years and seasons). As demonstrated, these factors have implications for the observed ranges of Mo- and U-EFs (Fig. 3B and C). Particularly, we identified the impact of a shallow SMTZ (high C/Sal ratio) in coastal depositional environments with an oxygenated water column as a key influence dictating the ability to differentiate between ir/regularly dysoxic and permanently oxic depositional environments. However, the statistical comparison of the violin plots demonstrates that when all sites are considered together, contrasts between redox bins are well reflected by Mo-EF, U-EF, or both, confirming the overall applicability of these proxies in coastal depositional environments. As a result, artefacts resulting from summarizing multiple depositional environments thus manifest as outliers around the expected trend controlled by redox conditions.

5.3.3. Normalizing TM enrichments against Al and the crustal background

The practice of normalizing TM enrichments against crustal background values is a topic of ongoing debate, due to potential overestimations of the authigenic signals. Several authors instead support the use of either "unnormalized" EFs, simply using the sample TM/Al ratio (Bennett and Canfield, 2020), or TM_{XS} using UCC and estimates of the local lithogenic background ratio in cases where TM_{XS} yields negative values (Jokinen et al., 2020). We compared the sequence of sites according to TM-EF values with the corresponding order according to TM/Al ratio and TM_{XS} (Figs. S5 + 6). The order of sites remained unchanged when using TM/Al ratios, due to the comparable calculation, and changed only slightly without improving the redox sequence when using TM_{XS}. A general issue that arises from using Al and crustal background values concerns depositional environments that are dominated by carbonates (marine or detrital), resulting in considerably lower Al contents compared to siliciclastic-dominated depositional environments. Consequently, if the chemical composition of the sediments largely varies across the study sites, then the resulting EFs become less comparable to each other, due to likely overestimations of the EFs at sites with lower Al (higher carbonate) contents. Certainly, more accurate results could be gathered from local background values, but these are often difficult to determine. Alternatively, average carbonate standards could provide a simpler solution (Steinmann et al., 2020). Although such carbonate standards exist (sedimentary carbonate rocks, deep-sea carbonates, Turekian and Wedepohl, 1961), the trace metal data are incomplete and subject to error. Essentially, as long as sites have a comparable chemical composition, this includes carbonate-rich sediments (e.g., Deng et al., 2020), normalization against the crustal background remains a valid tool. Among our study sites the chemical composition is relatively similar, except for the carbonate rich Black $Sea_{NW\ Abyssal\ Plain}$ site, which makes it principally less comparable to the other sites. These comparability issues arise both when using "unnormalized" EFs (sample TM/Al) and EFs using crustal background values. The reason is that while the particulate and sedimentary Mo and U concentrations of the river loads draining into the Black Sea are relatively close to UCC values (closer than to shale), Al contents are more similar to those of average deep-sea carbonates (Turekian and Wedepohl, 1961; Yigiterhan and Murray, 2008). Calculating EFs Black $Sea_{NW\ Abyssal\ Plain}$ site using UCC values for Mo and U, and deep-sea carbonate values for Al resulted in a considerably poorer differentiation of the redox bins 1 and 2–5 for both elements. Using unnormalized trace metal enrichments in this case might be the most suitable alternative for the Black Sea, but it might cause complications for sites with a larger detrital component of Mo and U. For the purpose of our study, focusing on mildly to non-reducing coastal depositional environments, largely with a heterogenous siliciclastic detrital background mixed, we found that using the UCC was the best approach.

5.3.4. Use of unnormalized trace metal threshold values

We further assessed the applicability of threshold TM content values to differentiate our defined redox bins. It has become a well-established approach to use a "universal" threshold value of unnormalized 25 ppm Mo as a baseline to differentiate non-euxinic from intermittently euxinic/ euxinic (paleo) redox environments, with data commonly displayed as histograms (Scott and Lyons, 2012; Dahl et al., 2013; Sweere et al., 2016; Scholz et al., 2017). As for Mo- and U-EFs, such thresholds must be applied with care due to the impact of secondary depositional environmental factors but provide a useful guide.

The majority of the samples of our sites in redox bins 1 and 2 have Mo contents between 10 and 50 ppm, with ~20% of the samples >50 ppm (Fig. 8A), which is generally in agreement with the findings by Scott and Lyons (2012). The relatively high occurrence of samples with Mo < 25 ppm in redox bins 1 and 2, however, leads to an overlap with samples from redox bins 3 and 4. The clearest differentiation in our dataset are samples where Mo >100 ppm, exclusively representing redox bin 1 (persistently euxinic). Contents of Mo >5 ppm are indicative of O_2

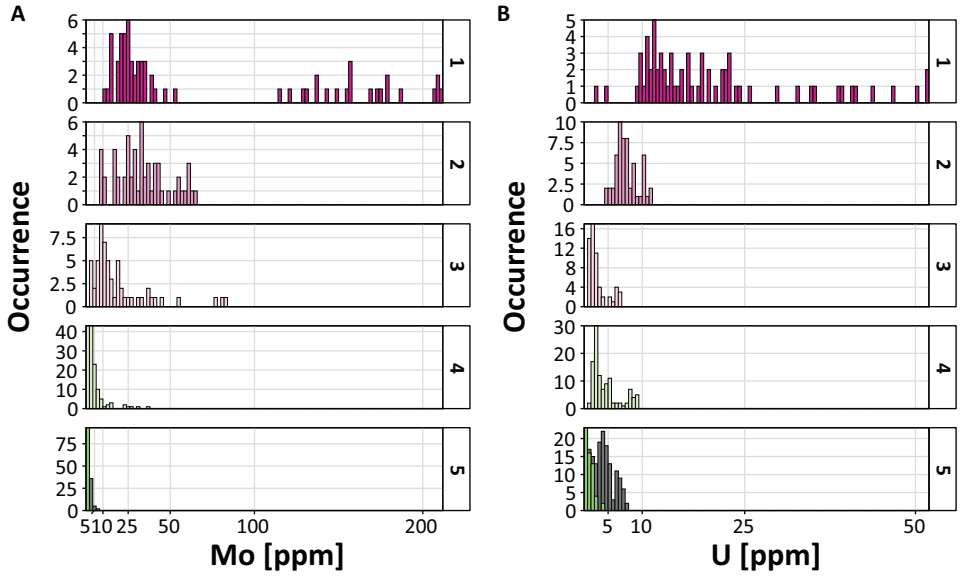

Fig. 8. Occurrence (histogram) distribution of unnormalized A) Mo and B) U concentrations for the different redox bins. The redox bins are indicated by their color and assigned redox bin numbers to the right of each panel. The vertical gray solid lines mark a selection of threshold values as defined in Scott and Lyons (2012) and Dahl et al., 2013). Data for samples from "fluffy" layers are not shown in this figure.

depletion corresponding to at least redox bin 3 (ir/regularly suboxic). Values of <5 ppm are observed only in redox bins 4 and 5 (ir/regularly dysoxic to persistently oxic). Differentiation between redox bins 4 and 5 is improved once the three oxic sites with a shallow SMTZ (high C/Sal ratio) are removed (gray shaded bars, Fig. 8A). A small overlap remains for values <1 ppm, however the majority of sites belong to redox bin 5. Overall, the histograms for Mo resemble Mo-EF violin plots in which redox bins 3–5 are clearly distinguishable in the frequency distribution.

For comparison, we followed the same threshold approach for U (Fig. 8B). In general, U enrichments of 5–10 ppm largely represent redox bin 2 sites, and values >10 ppm represent redox bin 1 sites, supporting the suggestion from the U-EF violin plot that U is a better redox proxy for differentiating between euxinic and ir/regularly euxinic environments. However, values <10 and < 5 cannot further distinguish between redox bins 3–5. As in the case for Mo-EF, this circumstance improves considerably once the three redox bin 5 sites are removed (gray shaded bars, Fig. 8B). In turn, redox bin 5 sites are more clearly recognizable by values <2 ppm. This finding supports our hypothesis that U, expressed as normalized EF or as unnormalized enrichments, is unable to reliably record bottom water redox changes in the range of oxic to ir/regularly suboxic, which contradicts the commonly accepted view of U as a more sensitive bottom water redox proxy than Mo. High C_{org} degradation and sulfide production rates, promoting higher U enrichments in oxic sites, may strongly weaken the sensitivity of U in more mildly reducing conditions. Despite showing similar discrepancies when using U-EFs, it must be noted that it is generally not advised to use unnormalized U contents due to having a larger detrital component compared to Mo, which dilutes the authigenic signal (here: 18 sites average $U_{detrital}$ = 46.4% of total U, $Mo_{detrital}$ = 25.7% of total Mo; Adams and Weaver, 1958; Cole et al., 2017). Ultimately, the total range within each redox bin provides more information on the impact of secondary factors, and mechanisms of Mo and U enrichments, than threshold values do.

6. Conclusions

Our study demonstrates that a combination of Mo- and U-Enrichment Factor (EF)-based redox proxies, supported by unnormalized molybdenum (Mo) and uranium (U) concentrations, allows differentiation of a variety of modern coastal depositional environments with regards to their bottom water O_2 conditions. In contrast to the common understanding, we found that Mo, rather than U, is the more sensitive and reliable bottom water redox proxy in mildly reducing depositional environments. At more severe levels of deoxygenation, U rather than Mo, is the more reliable proxy, owing to the relative insensitivity of U to factors limiting sedimentary enrichment in sulfidic depositional environments (i.e., "basin reservoir effect" and saturation limits). Through consideration of several secondary depositional environmental factors, we identified cases where the element-specific chemistry, shuttling of Mo with Fe (oxy)(hydr)oxides, depth of the sulfide front in the sediment, or a combination of these factors may obscure the relationship between redox conditions and Mo and U enrichments. We propose a scheme for assessing the potential impact of such secondary factors for Mo-and U-based redox proxy studies. Further studies should also address the potential role of grain size and sedimentary sources in influencing Mo- and U-EFs.

Declaration of Competing Interest

The authors declare that they have no known competing financial interests or personal relationships that could have appeared to influence the work reported in this paper.

Data availability

Research data are available in the Appendix A and upon request.

Acknowledgements

We thank the captain, crew, and scientific participants on board R/V Skagerrak (2019) and R/V Pelagia (2019) for their assistance with the field work campaigns. We acknowledge the staff of the Kristineberg Marine Research Station and the Royal Netherlands Institute for Sea Research (NIOZ) for their support during the field campaigns. The GeoLab, especially Helen de Waard, Coen Mulder, Natasja Welters, and Arnold van Dijk are acknowledged for analytical assistance at Utrecht University. We thank Heini Ali-Kovero for analytical assistance at the University of Helsinki. We also thank Martijn Hermans and Ricardo Correia for helping with making figures, computing in R, and providing feedback. This research was funded by the Academy of Finland (grant numbers 1319956 and 1345962). Additional funding was provided by

the Netherlands Organisation for Scientific Research (NWO; Vici-grant number 865.13.005), and the European Research Council (ERC Synergy Marix grant number 854088). This work was carried out under the program of the Netherlands Earth System Science Centre (NESSC), financially supported by the Ministry of Education, Culture and Science (OCW). HLF acknowledges support by the Swedish Research Council VR (grant number 2017-04190).

Appendix A. Supplementary data

Supplementary data to this article can be found online at https://doi.org/10.1016/j.chemgeo.2022.121203.

References

Adams, J.A., Weaver, C.E., 1958. Thorium-to-uranium ratios as indicators of sedimentary processes: example of concept of geochemical facies. AAPG Bull. 42 (2), 387–430.

Adelson, J.M., Helz, G.R., Miller, C.V., 2001. Reconstructing the rise of recent coastal anoxia; molybdenum in Chesapeake Bay sediments. Geochim. Cosmochim. Acta 65 (2), 237–252. https://doi.org/10.1016/S0016-7037(00)00539-1.

Alessi, D.S., Uster, B., Veeramani, H., Suvorova, E.I., Lezama-Pacheco, J.S., Stubbs, J.E., Bargar, J.R., Bernier-Latmani, R., 2012. Quantitative separation of monomeric U(IV) from UO2 in products of U(VI) reduction. Environ. Sci. Technol. 46 (11), 6150–6157. https://doi.org/10.1021/es204123z.

Algeo, T.J., 2004. Can marine anoxic events draw down the trace element inventory of seawater? Geology 32 (12). https://doi.org/10.1130/g20896.1.

Algeo, T.J., Li, C., 2020. Redox classification and calibration of redox thresholds in sedimentary systems. Geochim. Cosmochim. Acta 287, 8–26. https://doi.org/10.1016/j.gca.2020.01.055.

Algeo, T.J., Liu, J., 2020. A re-assessment of elemental proxies for paleoredox analysis. Chem. Geol. 540 https://doi.org/10.1016/j.chemgeo.2020.119549.

Algeo, T.J., Lyons, T.W., 2006. Mo-total organic carbon covariation in modern anoxic marine environments: Implications for analysis of paleoredox and paleohydrographic conditions. Paleoceanography 21 (1), PA1016. https://doi.org/10.1029/2004pa001112.

Algeo, T.J., Maynard, J.B., 2004. Trace-element behavior and redox facies in core shales of Upper Pennsylvanian Kansas-type cyclothems. Chem. Geol. 206 (3–4), 289–318. https://doi.org/10.1016/j.chemgeo.2003.12.009.

Algeo, T.J., Maynard, J.B., 2008. Trace-metal covariation as a guide to water-mass conditions in ancient anoxic marine environments. Geosphere 4 (5). https://doi.org/10.1130/ges00174.1.

Algeo, T.J., Rowe, H., 2012. Paleoceanographic applications of trace-metal concentration data. Chem. Geol. 324-325, 6–18. https://doi.org/10.1016/j.chemgeo.2011.09.002.

Algeo, T.J., Tribovillard, N., 2009. Environmental analysis of paleoceanographic systems based on molybdenum–uranium covariation. Chem. Geol. 268 (3–4), 211–225. https://doi.org/10.1016/j.chemgeo.2009.09.001.

Altieri, A.H., Harrison, S.B., Seemann, J., Collin, R., Diaz, R.J., Knowlton, N., 2017. Tropical dead zones and mass mortalities on coral reefs. Proc. Natl. Acad. Sci. U. S. A. 114 (14), 3660–3665. https://doi.org/10.1073/pnas.1621517114.

Anderson, R., LeHuray, A., Fleisher, M., Murray, J., 1989. Uranium deposition in saanich inlet sediments, Vancouver island. Geochim. Cosmochim. Acta 53 (9), 2205–2213. https://doi.org/10.1016/0016-7037(89)90344-X.

Anderson, R.F., Fleisher, M.O., 1991. Uranium Precipitation in Black-Sea Sediments. Black Sea Oceanogr. 351, 443–458. https://doi.org/10.1007/978-94-011-2608-3_26.

Bargar, J.R., Williams, K.H., Campbell, K.M., Long, P.E., Stubbs, J.E., Suvorova, E.I., Lezama-Pacheco, J.S., Alessi, D.S., Stylo, M., Webb, S.M., Davis, J.A., Giammar, D.E., Blue, L.Y., Bernier-Latmani, R., 2013. Uranium redox transition pathways in acetate-amended sediments. Proc. Natl. Acad. Sci. U. S. A. 110 (12), 4506–4511. https://doi.org/10.1073/pnas.1219198110.

Barnes, C.E., Cochran, J.K., 1991. Geochemistry of uranium in Black Sea sediments. Deep Sea Res. Part A 38, S1237–S1254. https://doi.org/10.1016/s0198-0149(10)80032-9.

Bennett, W.W., Canfield, D.E., 2020. Redox-sensitive trace metals as paleoredox proxies: a review and analysis of data from modern sediments. Earth Sci. Rev. 204 https://doi.org/10.1016/j.earscirev.2020.103175.

Bernier-Latmani, R., Veeramani, H., Vecchia, E.D., Junier, P., Lezama-Pacheco, J.S., Suvorova, E.I., Sharp, J.O., Wigginton, N.S., Bargar, J.R., 2010. Non-uraninite Products of Microbial U(VI) reduction. Environ. Sci. Technol. 44 (24), 9456–9462. https://doi.org/10.1021/es101675a.

Berrang, P., Grill, E., 1974. The effect of manganese oxide scavenging on molybdenum in Saanich Inlet, British Columbia. Mar. Chem. 2 (2), 125–148.

Bertine, K.K., Turekian, K.K., 1973. Molybdenum in Marine Deposits. Geochim. Cosmochim. Acta 37 (6), 1415–1434. https://doi.org/10.1016/0016-7037(73)90080-X.

Bindoff, N.L., Cheung, W.W.L., Kairo, J.G., Arístegui, J., Guinder, V.A., Hallberg, R., Hilmi, N., Jiao, N., Karim, M.S., Levin, L., O'Donoghue, S., Purca Cuicapusa, S.R., Rinkevich, B., Suga, T., Tagliabue, A., Williamson, P., 2019. Changing Ocean, Marine Ecosystems, and Dependent Communities, IPCC Special Report on the Ocean and Cryosphere in a Changing Climate. Cambridge University Press, Cambridge, UK and New York, NY, USA, pp. 477–587. https://doi.org/10.1017/9781009157964.007.

Boetius, A., Ravenschlag, K., Schubert, C.J., Rickert, D., Widdel, F., Gieseke, A., Amann, R., Jorgensen, B.B., Witte, U., Pfannkuche, O., 2000. A marine microbial consortium apparently mediating anaerobic oxidation of methane. Nature 407 (6804), 623–626. https://doi.org/10.1038/35036572.

Bonatti, E., Fisher, D., Joensuu, O., Rydell, H., 1971. Postdepositional mobility of some transition elements, phosphorus, uranium and thorium in deep sea sediments. Geochim. Cosmochim. Acta 35 (2), 189–201.

Bone, S.E., Dynes, J.J., Cliff, J., Bargar, J.R., 2017. Uranium(IV) adsorption by natural organic matter in anoxic sediments. Proc. Natl. Acad. Sci. U. S. A. 114 (4), 711–716. https://doi.org/10.1073/pnas.1611918114.

Breitburg, D., Levin, L.A., Oschlies, A., Gregoire, M., Chavez, F.P., Conley, D.J., Garcon, V., Gilbert, D., Gutierrez, D., Isensee, K., Jacinto, G.S., Limburg, K.E., Montes, I., Naqvi, S.W.A., Pitcher, G.C., Rabalais, N.N., Roman, M.R., Rose, K.A., Seibel, B.A., Telszewski, M., Yasuhara, M., Zhang, J., 2018. Declining oxygen in the global ocean and coastal waters. Science 359 (6371). https://doi.org/10.1126/science.aam7240.

Brennecka, G.A., Wasylenki, L.E., Bargar, J.R., Weyer, S., Anbar, A.D., 2011. Uranium Isotope Fractionation during Adsorption to Mn-Oxyhydroxides. Environ. Sci. Technol. 45 (4), 1370–1375. https://doi.org/10.1021/es103061v.

Brinkmann, I., Barras, C., Jilbert, T., Naeraa, T., Paul, K.M., Schweizer, M., Filipsson, H. L., 2021. Drought recorded by Ba/ca in coastal benthic foraminifera. Biogeosci. Discuss. 2021, 1–23. https://doi.org/10.5194/bg-2021-310.

Brumsack, H.-J., 2006. The trace metal content of recent organic carbon-rich sediments: Implications for cretaceous black shale formation. Palaeogeogr. Palaeoclimatol. Palaeoecol. 232 (2–4), 344–361. https://doi.org/10.1016/j.palaeo.2005.05.011.

Bura-Nakić, E., Sondi, I., Mikac, N., Andersen, M.B., 2020. Investigating the molybdenum and uranium redox proxies in a modern shallow anoxic carbonate rich marine sediment setting of the Malo Jezero (Mljet Lakes, Adriatic Sea). Chem. Geol. 533 https://doi.org/10.1016/j.chemgeo.2019.119441.

Burdige, D.J., 2006. Geochemistry of Marine Sediments. Princeton University Press. https://doi.org/10.2307/j.ctv131bw7s.

Calvert, S.E., Pedersen, T.F., 1993. Geochemistry of recent Oxic and Anoxic Marine-Sediments - Implications for the Geological Record. Mar. Geol. 113 (1–2), 67–88. https://doi.org/10.1016/0025-3227(93)90150-T.

Canfield, D.E., Thamdrup, B., Hansen, J.W., 1993. The anaerobic degradation of organic matter in Danish coastal sediments: Iron reduction, manganese reduction, and sulfate reduction. Geochim. Cosmochim. Acta 57 (16), 3867–3883. https://doi.org/10.1016/0016-7037(93)90340-3.

Carpenter, J., Bithell, J., 2000. Bootstrap confidence intervals: when, which, what? A practical guide for medical statisticians. Stat. Med. 19 (9), 1141–1164. https://doi.org/10.1002/(sici)1097-0258(20000515)19:9<1141::aid-sim479>3.0.co;2-f.

Carstensen, J., Conley, D.J., Bonsdorff, E., Gustafsson, B.G., Hietanen, S., Janas, U., Jilbert, T., Maximov, A., Norkko, A., Norkko, J., Reed, D.C., Slomp, C.P., Timmermann, K., Voss, M., 2014. Hypoxia in the Baltic Sea: biogeochemical cycles, benthic fauna, and management. Ambio 43 (1), 26–36. https://doi.org/10.1007/s13280-013-0474-7.

Cochran, J.K., Carey, A.E., Sholkovitz, E.R., Surprenant, L.D., 1986. The Geochemistry of Uranium and Thorium in Coastal Marine-Sediments and Sediment Pore Waters. Geochim. Cosmochim. Acta 50 (5), 663–680. https://doi.org/10.1016/0016-7037(86)90344-3.

Cole, D.B., Zhang, S., Planavsky, N.J., 2017. A new estimate of detrital redox-sensitive metal concentrations and variability in fluxes to marine sediments. Geochim. Cosmochim. Acta 215, 337–353. https://doi.org/10.1016/j.gca.2017.08.004.

Conley, D.J., Carstensen, J., Aigars, J., Axe, P., Bonsdorff, E., Eremina, T., Haahti, B.M., Humborg, C., Jonsson, P., Kotta, J., Lannegren, C., Larsson, U., Maximov, A., Medina, M.R., Lysiak-Pastuszak, E., Remeikaite-Nikiene, N., Walve, J., Wilhelms, S., Zillen, L., 2011. Hypoxia is increasing in the coastal zone of the Baltic Sea. Environ. Sci. Technol. 45 (16), 6777–6783. https://doi.org/10.1021/es201212r.

Crusius, J., Calvert, S., Pedersen, T., Sage, D., 1996. Rhenium and molybdenum enrichments in sediments as indicators of oxic, suboxic and sulfidic conditions of deposition. Earth Planet. Sci. Lett. 145 (1–4), 65–78. https://doi.org/10.1016/S0012-821x(96)00204-X.

Curtis, C.D., 1966. The incorporation of soluble organic matter into sediments and its effect on trace-element assemblages. In: Hobsen, G.D., Louis, M.C. (Eds.), Advances in Organic Geochemistry, 1964. Proc. Int. Meet., Rueil-Malmaison. Pergamond Press, pp. 1–13. https://doi.org/10.1016/B978-0-08-011577-1.50004-1.

Dahl, T.W., Chappaz, A., Fitts, J.P., Lyons, T.W., 2013. Molybdenum reduction in a sulfidic lake: evidence from X-ray absorption fine-structure spectroscopy and implications for the Mo paleoproxy. Geochim. Cosmochim. Acta 103, 213–231. https://doi.org/10.1016/j.gca.2012.10.058.

Dalcin Martins, P., de Monlevad, J.P.R.C., Lenstra, W.K., Wallenius, A.J., Echeveste Medrano, M.J., Hermans, M., Slomp, C.P., Welte, C.U., Jetten, M.S.M., van Helmond, N.A.G.M., 2022. Sulfide toxicity as key control on anaerobic oxidation of methane in eutrophic coastal sediments. bioRxiv. https://doi.org/10.1101/2022.02.10.479873.

Dang, D.H., Novotnik, B., Wang, W., Georg, R.B., Evans, R.D., 2016. Uranium Isotope Fractionation during Adsorption, (Co)precipitation, and Biotic Reduction. Environ. Sci. Technol. 50 (23), 12695–12704. https://doi.org/10.1021/acs.est.6b01459.

Dellwig, O., Wegwerth, A., Arz, H.W., 2021. Anatomy of the Major Baltic Inflow in 2014: Impact of manganese and iron shuttling on phosphorus and trace metals in the Gotland Basin, Baltic Sea. Cont. Shelf Res. 223 https://doi.org/10.1016/j.csr.2021.104449.

Deng, Y.N., Chen, F., Hu, Y., Guo, Q.J., Cao, J., Chen, H., Zhou, J.H., Jiang, X.X., Zhu, J., 2020. Methane seepage patterns during the middle Pleistocene inferred from molybdenum enrichments of seep carbonates in the South China Sea. Ore Geol. Rev. 125 https://doi.org/10.1016/j.oregeorev.2020.103701.

Diaz, R., Rosenberg, R., Sturdivant, K., 2019. Hypoxia in Estuaries and Semi-Enclosed Seas, Ocean Deoxygenation: Everyone's Problem, Ed. Laffoley, D. and Baxter, JM, IUCN, Gland, Switzerland, doi: https://doi.org/10.2305/IUCN.CH.2019.13.en.

Diaz, R.J., Rosenberg, R., 1995. Marine benthic hypoxia: a review of its ecological effects and the behavioural responses of benthic macrofauna. Oceanogr. Mar. Biol. 33, 245–303.

Diaz, R.J., Rosenberg, R., 2008. Spreading dead zones and consequences for marine ecosystems. Science 321 (5891), 926–929. https://doi.org/10.1126/science.1156401.

Dijkstra, N., Kraal, P., Séguret, M.J.M., Flores, M.R., Gonzalez, S., Rijkenberg, M.J.A., Slomp, C.P., 2018. Phosphorus dynamics in and below the redoxcline in the Black Sea and implications for phosphorus burial. Geochim. Cosmochim. Acta 222, 685–703. https://doi.org/10.1016/j.gca.2017.11.016.

Dorta, C.C., Rona, E., 1971. Geochemistry of Uranium in Cariaco Trench. B Mar Sci 21 (3), 754–765.

Dunk, R.M., Mills, R.A., Jenkins, W.J., 2002. A reevaluation of the oceanic uranium budget for the Holocene. Chem. Geol. 190 (1–4), 45–67. https://doi.org/10.1016/S0009-2541(02)00110-9.

EEA, 2019. Trends in dissolved oxygen concentrations. In: European Environment Agency (EEA). https://www.eea.europa.eu/data-and-maps/indicators/oxygen-concentrations-in-coastal-and/assessment. last accessed: 28 January 2022.

Egger, M., Rasigraf, O., Sapart, C.J., Jilbert, T., Jetten, M.S., Rockmann, T., van der Veen, C., Banda, N., Kartal, B., Ettwig, K.F., Slomp, C.P., 2015. Iron-mediated anaerobic oxidation of methane in brackish coastal sediments. Environ. Sci. Technol. 49 (1), 277–283. https://doi.org/10.1021/es503663z.

Erickson, B.E., Helz, G.R., 2000. Molybdenum(VI) speciation in sulfidic waters: Stability and lability of thiomolybdates. Geochim. Cosmochim. Acta 64 (7), 1149–1158. https://doi.org/10.1016/S0016-7037(99)00423-8.

Filipsson, H.L., Nordberg, K., 2004. A 200-year environmental record of a low-oxygen fjord, Sweden, elucidated by benthic foraminifera, sediment characteristics and hydrographic data. J. Foramin. Res. 34 (4), 277–293. https://doi.org/10.2113/34.4.277.

Fleming-Lehtinen, V., Raike, A., Kortelainen, P., Kauppila, P., Thomas, D.N., 2015. Organic Carbon Concentration in the Northern Coastal Baltic Sea between 1975 and 2011. Estuar. Coasts 38 (2), 466–481. https://doi.org/10.1007/s12237-014-9829-y.

Garrels, R.M., 1955. Some thermodynamic relations among the uranium oxides and their relation to the oxidation states of the uranium ores of the Colorado Plateaus. Am. Mineral. 40 (11−12), 1004–1021. https://doi.org/10.3133/TEI455.

Glud, R.N., Holby, O., Hoffmann, F., Canfield, D.E., 1998. Benthic mineralization and exchange in Arctic sediments (Svalbard, Norway). Mar. Ecol. Prog. Ser. 173, 237–251. https://doi.org/10.3354/meps173237.

Goldberg, T., Archer, C., Vance, D., Thamdrup, B., McAnena, A., Poulton, S.W., 2012. Controls on Mo isotope fractionations in a Mn-rich anoxic marine sediment, Gullmar Fjord, Sweden. Chem. Geol. 296, 73–82. https://doi.org/10.1016/j.chemgeo.2011.12.020.

Gooday, A.J., Jorissen, F., Levin, L.A., Middelburg, J.J., Naqvi, S.W.A., Rabalais, N.N., Scranton, M., Zhang, J., 2009. Historical records of coastal eutrophication-induced hypoxia. Biogeosciences 6 (8), 1707–1745. https://doi.org/10.5194/bg-6-1707-2009.

Grégoire, M., Garcon, V., Garcia, H., Breitburg, D., Isensee, K., Oschlies, A., Telszewski, M., Barth, A., Bittig, H.C., Carstensen, J., Carval, T., Chai, F., Chavez, F., Conley, D., Coppola, L., Crowe, S., Currie, K., Dai, M.H., Deflandre, B., Dewitte, B., Diaz, R., Garcia-Robledo, E., Gilbert, D., Giorgetti, A., Glud, R., Gutierrez, D., Hosoda, S., Ishii, M., Jacinto, G., Langdon, C., Lauvset, S.K., Levin, L.A., Limburg, K. E., Mehrtens, H., Montes, I., Naqvi, W., Paulmier, A., Pfeil, B., Pitcher, G., Pouliquen, S., Rabalais, N., Rabouille, C., Recape, V., Roman, M., Rose, K., Rudnick, D., Rummer, J., Schmechtig, C., Schmidtko, S., Seibel, B., Slomp, C., Sumalia, U.R., Tanhua, T., Thierry, V., Uchida, H., Wanninkhof, R., Yasuhara, M., 2021. A Global Ocean Oxygen Database and Atlas for Assessing and predicting Deoxygenation and Ocean Health in the Open and Coastal Ocean. Front. Mar. Sci. 8 https://doi.org/10.3389/fmars.2021.724913.

Hagens, M., Slomp, C.P., Meysman, F.J.R., Seitaj, D., Harlay, J., Borges, A.V., Middelburg, J.J., 2015. Biogeochemical processes and buffering capacity concurrently affect acidification in a seasonally hypoxic coastal marine basin. Biogeosciences 12 (5), 1561–1583. https://doi.org/10.5194/bg-12-1561-2015.

Hallberg, R.O., 1974. Paleoredox conditions in the Eastern Gotland Basin during the recent centuries. Merentutkimuslaitoksen Julk. Havsforskningsinst. Skr. 238, 3–16.

Helly, J.J., Levin, L.A., 2004. Global distribution of naturally occurring marine hypoxia on continental margins. Deep-Sea Res. I Oceanogr. Res. Pap. 51 (9), 1159–1168. https://doi.org/10.1016/j.dsr.2004.03.009.

van Helmond, N.A.G.M., Jilbert, T., Slomp, C.P., 2018. Hypoxia in the Holocene Baltic Sea: comparing modern versus past intervals using sedimentary trace metals. Chem. Geol. 493, 478–490. https://doi.org/10.1016/j.chemgeo.2018.06.028.

Helz, G., Miller, C., Charnock, J., Mosselmans, J., Pattrick, R., Garner, C., Vaughan, D., 1996. Mechanism of molybdenum removal from the sea and its concentration in black shales: EXAFS evidence. Geochim. Cosmochim. Acta 60 (19), 3631–3642.

Helz, G.R., 2021. Dissolved molybdenum asymptotes in sulfidic waters. Geochem. Perspect. Lett. 19, 23–26. https://doi.org/10.7185/geochemlet.2129.

Helz, G.R., Vorlicek, T.P., 2019. Precipitation of molybdenum from euxinic waters and the role of organic matter. Chem. Geol. 509, 178–193. https://doi.org/10.1016/j.chemgeo.2019.02.001.

Hermans, M., Lenstra, W.K., Hidalgo-Martinez, S., van Helmond, N.A.G.M., Witbaard, R., Meysman, F.J.R., Gonzalez, S., Slomp, C.P., 2019a. Abundance and Biogeochemical Impact of Cable Bacteria in Baltic Sea Sediments. Environ. Sci. Technol. 53 (13), 7494–7503. https://doi.org/10.1021/acs.est.9b01665.

Hermans, M., Lenstra, W.K., van Helmond, N.A.G.M., Behrends, T., Egger, M., Séguret, M.J.M., Gustafsson, E., Gustafsson, B.G., Slomp, C.P., 2019b. Impact of natural re-oxygenation on the sediment dynamics of manganese, iron and phosphorus in a euxinic Baltic Sea basin. Geochim. Cosmochim. Acta 246, 174–196. https://doi.org/10.1016/j.gca.2018.11.033.

Hermans, M., Risgaard-Petersen, N., Meysman, F.J.R., Slomp, C.P., 2020. Biogeochemical impact of cable bacteria on coastal Black Sea sediment. Biogeosciences 17 (23), 5919–5938. https://doi.org/10.5194/bg-17-5919-2020.

Hertta, 2021. Water Quality Monitoring Data 1974-2019. Environmental information systems / Water quality SYKE (Finnish Environment Institute). https://www.syke.fi/fi-FI/Avoin_tieto/Ymparistotietojarjestelmat. last accessed: 9 February 2022.

Hinrichs, J., 2001. Geochemical tracers in the deep-sea and the North Sea. Universität Oldenburg. https://oops.uni-oldenburg.de/id/eprint/322.

Hirose, K., Sugimura, Y., 1991. Chemical Speciation of Particulate Uranium in Seawater. J. Radioanal. Nucl. Chem. 149 (1), 83–96. https://doi.org/10.1007/Bf02053716.

Jacobs, L., Emerson, S., Skei, J., 1985. Partitioning and Transport of Metals across the O2/H2s Interface in a Permanently Anoxic Basin - Framvaren Fjord, Norway. Geochim. Cosmochim. Acta 49 (6), 1433–1444. https://doi.org/10.1016/0016-7037(85)90293-5.

Jilbert, T., Slomp, C.P., 2013a. Rapid high-amplitude variability in Baltic Sea hypoxia during the Holocene. Geology 41 (11), 1183–1186. https://doi.org/10.1130/g34804.1.

Jilbert, T., Slomp, C.P., 2013b. Iron and manganese shuttles control the formation of authigenic phosphorus minerals in the euxinic basins of the Baltic Sea. Geochim. Cosmochim. Acta 107, 155–169. https://doi.org/10.1016/j.gca.2013.01.005.

Jilbert, T., Slomp, C.P., Gustafsson, B.G., Boer, W., 2011. Beyond the Fe-P-redox connection: preferential regeneration of phosphorus from organic matter as a key control on Baltic Sea nutrient cycles. Biogeosciences 8 (6), 1699–1720. https://doi.org/10.5194/bg-8-1699-2011.

Jilbert, T., Asmala, E., Schröder, C., Tiihonen, R., Myllykangas, J.-P., Virtasalo, J.J., Kotilainen, A., Peltola, P., Ekholm, P., Hietanen, S., 2018. Impacts of flocculation on the distribution and diagenesis of iron in boreal estuarine sediments. Biogeosciences 15 (4), 1243–1271. https://doi.org/10.5194/bg-15-1243-2018.

Jokinen, S.A., Virtasalo, J.J., Kotilainen, A.T., Saarinen, T., 2015. Varve microfabric record of seasonal sedimentation and bottom flow-modulated mud deposition in the coastal northern Baltic Sea. Mar. Geol. 366, 79–96. https://doi.org/10.1016/j.margeo.2015.05.003.

Jokinen, S.A., Koho, K., Virtasalo, J.J., Jilbert, T., 2020. Depth and intensity of the sulfate-methane transition zone control sedimentary molybdenum and uranium sequestration in a eutrophic low-salinity setting. Appl. Geochem. 122 https://doi.org/10.1016/j.apgeochem.2020.104767.

Jørgensen, B.B., Glud, R.N., Holby, O., 2005. Oxygen distribution and bioirrigation in Arctic fjord sediments (Svalbard, Barents Sea). Mar. Ecol. Prog. Ser. 292, 85–95. https://doi.org/10.3354/meps292085.

Jørgensen, B.B., Beulig, F., Egger, M., Petro, C., Scholze, C., Røy, H., 2019. Organoclastic sulfate reduction in the sulfate-methane transition of marine sediments. Geochim. Cosmochim. Acta 254, 231–245. https://doi.org/10.1016/j.gca.2019.03.016.

Keeling, R.F., Kortzinger, A., Gruber, N., 2010. Ocean Deoxygenation in a Warming World. Annu. Rev. Mar. Sci. 2, 199–229. https://doi.org/10.1146/annurev.marine.010908.163855.

Klinkhammer, G.P., Palmer, M.R., 1991. Uranium in the Oceans - where it Goes and why. Geochim. Cosmochim. Acta 55 (7), 1799–1806. https://doi.org/10.1016/0016-7037(91)90024-Y.

Koczy, F.F., Tomic, E., Hecht, F., 1957. Zur Geochemie Des Urans Im Ostseebecken. Geochim. Cosmochim. Acta 11 (1–2), 86–102. https://doi.org/10.1016/0016-7037(57)90007-8.

Kraal, P., Dijkstra, N., Behrends, T., Slomp, C.P., 2017. Phosphorus burial in sediments of the sulfidic deep Black Sea: Key roles for adsorption by calcium carbonate and apatite authigenesis. Geochim. Cosmochim. Acta 204, 140–158. https://doi.org/10.1016/j.gca.2017.01.042.

Langmuir, D., 1978. Uranium solution-mineral equilibria at low temperatures with applications to sedimentary ore deposits. Geochim. Cosmochim. Acta 42 (6), 547–569.

Lee, S.Y., Cha, W.S., Kim, J.-G., Baik, M.H., Jung, E.C., Jeong, J.T., Kim, K., Chung, S.Y., Lee, Y.J., 2014. Uranium(IV) remobilization under sulfate reducing conditions. Chem. Geol. 370, 40–48. https://doi.org/10.1016/j.chemgeo.2014.01.020.

Lenstra, W.K., Hermans, M., Séguret, M.J.M., Witbaard, R., Behrends, T., Dijkstra, N., van Helmond, N.A.G.M., Kraal, P., Laan, P., Rijkenberg, M.J.A., Severmann, S., Teacă, A., Slomp, C.P., 2019. The shelf-to-basin iron shuttle in the Black Sea revisited. Chem. Geol. 511, 314–341. https://doi.org/10.1016/j.chemgeo.2018.10.024.

Lenz, C., Jilbert, T., Conley, D.J., Wolthers, M., Slomp, C.P., 2015. Are recent changes in sediment manganese sequestration in the euxinic basins of the Baltic Sea linked to the expansion of hypoxia? Biogeosciences 12 (16), 4875–4894. https://doi.org/10.5194/bg-12-4875-2015.

Levin, L.A., Ekau, W., Gooday, A.J., Jorissen, F., Middelburg, J.J., Naqvi, S.W.A., Neira, C., Rabalais, N.N., Zhang, J., 2009. Effects of natural and human-induced hypoxia on coastal benthos. Biogeosciences 6 (10), 2063–2098. https://doi.org/10.5194/bg-6-2063-2009.

Little, S.H., Vance, D., Lyons, T.W., McManus, J., 2015. Controls on trace metal authigenic enrichment in reducing sediments: Insights from modern oxygen-deficient settings. Am. J. Sci. 315 (2), 77–119. https://doi.org/10.2475/02.2015.01.

Liu, J., Algeo, T.J., 2020. Beyond redox: Control of trace-metal enrichment in anoxic marine facies by watermass chemistry and sedimentation rate. Geochim. Cosmochim. Acta 287, 296–317. https://doi.org/10.1016/j.gca.2020.02.037.

Lovley, D.R., Phillips, E.J.P., Gorby, Y.A., Landa, E.R., 1991. Microbial Reduction of Uranium. Nature 350 (6317), 413–416. https://doi.org/10.1038/350413a0.
Lovley, D.R., Roden, E.E., Phillips, E.J.P., Woodward, J.C., 1993. Enzymatic Iron and Uranium Reduction by Sulfate-reducing Bacteria. Mar. Geol. 113 (1–2), 41–53. https://doi.org/10.1016/0025-3227(93)90148-O.
Lyons, T.W., Kashgarian, M., 2005. Paradigm lost, Paradigm Found: the Black Sea-Black Shale connection as Viewed from the Anoxic Basin margin. Oceanography 18 (2), 86–99. https://doi.org/10.5670/OCEANOG.2005.44.
Malkin, S.Y., Rao, A.M.F., Seitaj, D., Vasquez-Cardenas, D., Zetsche, E.M., Hidalgo-Martinez, S., Boschker, H.T.S., Meysman, F.J.R., 2014. Natural occurrence of microbial Sulphur oxidation by long-range electron transport in the seafloor (vol 8, pg 1843, 2014). ISME J. 8 (12), 2551–2552. https://doi.org/10.1038/ismej.2014.170.
Manheim, F.T., 1961. A Geochemical Profile in the Baltic Sea. Geochim. Cosmochim. Acta 25 (1), 52–70. https://doi.org/10.1016/0016-7037(61)90059-X.
Martin, W., Sayles, F., 1987. Seasonal cycles of particle and solute transport processes in nearshore sediments: 222Rn226Ra and 234Th238U disequilibrium at a site in Buzzards Bay, MA. Geochim. Cosmochim. Acta 51 (4), 927–943.
McLennan, S.M., 2001. Relationships between the trace element composition of sedimentary rocks and upper continental crust. Geochem. Geophys. Geosyst. 2 https://doi.org/10.1029/2000gc000109.
McManus, J., Berelson, W.M., Klinkhammer, G.P., Hammond, D.E., Holm, C., 2005. Authigenic uranium: Relationship to oxygen penetration depth and organic carbon rain. Geochim. Cosmochim. Acta 69 (1), 95–108. https://doi.org/10.1016/j.gca.2004.06.023.
Miller, C.A., Peucker-Ehrenbrink, B., Walker, B.D., Marcantonio, F., 2011. Re-assessing the surface cycling of molybdenum and rhenium. Geochim. Cosmochim. Acta 75 (22), 7146–7179. https://doi.org/10.1016/j.gca.2011.09.005.
Morford, J.L., Emerson, S.R., Breckel, E.J., Kim, S.H., 2005. Diagenesis of oxyanions (V, U, Re, and Mo) in pore waters and sediments from a continental margin. Geochim. Cosmochim. Acta 69 (21), 5021–5032. https://doi.org/10.1016/j.gca.2005.05.015.
Morford, J.L., Martin, W.R., Carney, C.M., 2009a. Uranium diagenesis in sediments underlying bottom waters with high oxygen content. Geochim. Cosmochim. Acta 73 (10), 2920–2937. https://doi.org/10.1016/j.gca.2009.02.014.
Morford, J.L., Martin, W.R., François, R., Carney, C.M., 2009b. A model for uranium, rhenium, and molybdenum diagenesis in marine sediments based on results from coastal locations. Geochim. Cosmochim. Acta 73 (10), 2938–2960. https://doi.org/10.1016/j.gca.2009.02.029.
Mort, H.P., Slomp, C.P., Gustafsson, B.G., Andersen, T.J., 2010. Phosphorus recycling and burial in Baltic Sea sediments with contrasting redox conditions. Geochim. Cosmochim. Acta 74 (4), 1350–1362. https://doi.org/10.1016/j.gca.2009.11.016.
Murray, J.W., Top, Z., Ozsoy, E., 1991. Hydrographic Properties and Ventilation of the Black-Sea. Deep Sea Res. Part A 38, S663–S689. https://doi.org/10.1016/S0198-0149(10)80003-2.
Myllykangas, J.P., Hietanen, S., Jilbert, T., 2020. Legacy Effects of Eutrophication on Modern methane Dynamics in a Boreal Estuary. Estuar. Coasts 43 (2), 189–206. https://doi.org/10.1007/s12237-019-00677-0.
Naqvi, S.W.A., Bange, H.W., Farias, L., Monteiro, P.M.S., Scranton, M.I., Zhang, J., 2010. Marine hypoxia/anoxia as a source of CH4 and N2O. Biogeosciences 7 (7), 2159–2190. https://doi.org/10.5194/bg-7-2159-2010.
Noordmann, J., Weyer, S., Montoya-Pino, C., Dellwig, O., Neubert, N., Eckert, S., Paetzel, M., Böttcher, M.E., 2015. Uranium and molybdenum isotope systematics in modern euxinic basins: Case studies from the Central Baltic Sea and the Kyllaren fjord (Norway). Chem. Geol. 396, 182–195. https://doi.org/10.1016/j.chemgeo.2014.12.012.
Nordberg, K., Filipsson, H.L., Gustafsson, M., Harland, R., Roos, P., 2001. Climate, hydrographic variations and marine benthic hypoxia in Koljö Fjord, Sweden. J. Sea Res. 46 (3–4), 187–200. https://doi.org/10.1016/S1385-1101(01)00084-3.
Pham-Gia, T., Hung, T.L., 2001. The mean and median absolute deviations. Math. Comput. Model. 34 (7–8), 921–936. https://doi.org/10.1016/S0895-7177(01)00109-1.
Pilipchuk, M., Volkov, I., 1974. Behavior of molybdenum in processes of sediment formation and diagenesis in Black Sea. Geochemistry. https://doi.org/10.1306/M20377C17.
Presley, B.J., Nissenbaum, A., Kaplan, I.R., Kolodny, Y., 1972. Early Diagenesis in a Reducing Fjord, Saanich Inlet, British-Columbia .2. Trace-Element Distribution in Interstitial Water and Sediment. Geochim. Cosmochim. Acta 36 (10), 1073–1090. https://doi.org/10.1016/0016-7037(72)90092-0.
Rabalais, N.N., Diaz, R.J., Levin, L.A., Turner, R.E., Gilbert, D., Zhang, J., 2010. Dynamics and distribution of natural and human-caused hypoxia. Biogeosciences 7 (2), 585–619. https://doi.org/10.5194/bg-7-585-2010.
Reimann, C., De Caritat, P., 2000. Intrinsic flaws of element enrichment factors (EFs) in environmental geochemistry. Environ. Sci. Technol. 34 (24), 5084–5091. https://doi.org/10.1021/es001339o.
Reimann, C., de Caritat, P., 2005. Distinguishing between natural and anthropogenic sources for elements in the environment: regional geochemical surveys versus enrichment factors. Sci. Total Environ. 337 (1–3), 91–107. https://doi.org/10.1016/j.scitotenv.2004.06.011.
Rickard, D., Luther, G.W., 2007. Chemistry of iron sulfides. Chem. Rev. 107 (2), 514–562. https://doi.org/10.1021/cr0503658.
Rijkswaterstaat, 2020. Water Chemistry Data 1978–2020. Ministerie van Infrastructuur en Waterstaat. https://www.deltaexpertise.nl/grevelingen/systeemrapportage/zuurstofUitTSO.html#zuurstofUitTSO.
Rowland, J.A., Bland, L.M., James, S., Nicholson, E., 2021. A guide to representing variability and uncertainty in biodiversity indicators. Conserv. Biol. 35 (5), 1669–1682. https://doi.org/10.1111/cobi.13699.
Rudnick, R.L., Gao, S., 2014. Composition of the Continental Crust, Treatise on Geochemistry, pp. 1–51. https://doi.org/10.1016/b978-0-08-095975-7.00301-6.
Scholz, F., McManus, J., Sommer, S., 2013. The manganese and iron shuttle in a modern euxinic basin and implications for molybdenum cycling at euxinic ocean margins. Chem. Geol. 355, 56–68. https://doi.org/10.1016/j.chemgeo.2013.07.006.
Scholz, F., Severmann, S., McManus, J., Noffke, A., Lomnitz, U., Hensen, C., 2014. On the isotope composition of reactive iron in marine sediments: Redox shuttle versus early diagenesis. Chem. Geol. 389, 48–59. https://doi.org/10.1016/j.chemgeo.2014.09.009.
Scholz, F., Siebert, C., Dale, A.W., Frank, M., 2017. Intense molybdenum accumulation in sediments underneath a nitrogenous water column and implications for the reconstruction of paleo-redox conditions based on molybdenum isotopes. Geochim. Cosmochim. Acta 213, 400–417. https://doi.org/10.1016/j.gca.2017.06.048.
Scott, C., Lyons, T.W., 2012. Contrasting molybdenum cycling and isotopic properties in euxinic versus non-euxinic sediments and sedimentary rocks: refining the paleoproxies. Chem. Geol. 324-325, 19–27. https://doi.org/10.1016/j.chemgeo.2012.05.012.
Seitaj, D., Schauer, R., Sulu-Gambari, F., Hidalgo-Martinez, S., Malkin, S.Y., Burdorf, L.D.W., Slomp, C.P., Meysman, F.J.R., 2015. Cable bacteria generate a firewall against euxinia in seasonally hypoxic basins. Proc. Natl. Acad. Sci. U. S. A. 112 (43), 13278–13283. https://doi.org/10.1073/pnas.1510152112.
Sharp, J.O., Lezama-Pacheco, J.S., Schofield, E.J., Junier, P., Ulrich, K.-U., Chinni, S., Veeramani, H., Margot-Roquier, C., Webb, S.M., Tebo, B.M., Giammar, D.E., Bargar, J.R., Bernier-Latmani, R., 2011. Uranium speciation and stability after reductive immobilization in aquifer sediments. Geochim. Cosmochim. Acta 75 (21), 6497–6510. https://doi.org/10.1016/j.gca.2011.08.022.
Shaw, T.J., Sholkovitz, E.R., Klinkhammer, G., 1994. Redox Dynamics in the Chesapeake Bay - the effect on Sediment-Water Uranium Exchange. Geochim. Cosmochim. Acta 58 (14), 2985–2995. https://doi.org/10.1016/0016-7037(94)90173-2.
Singh, A., Catalano, J.G., Ulrich, K.U., Giammar, D.E., 2012. Molecular-Scale Structure of Uranium(VI) Immobilized with Goethite and Phosphate. Environ. Sci. Technol. 46 (12), 6594–6603. https://doi.org/10.1021/es300494x.
Slomp, C.P., Mort, H.P., Jilbert, T., Reed, D.C., Gustafsson, B.G., Wolthers, M., 2013. Coupled Dynamics of Iron and Phosphorus in Sediments of an Oligotrophic Coastal Basin and the Impact of Anaerobic Oxidation of methane. PLoS One 8 (4). https://doi.org/10.1371/journal.pone.0062386.
SMHI, 2020. Water chemistry data 1960–2019. In: Svenskt HavsARKivs (SHARK) hydrdographic database Swedish Meteorological and Hydrological Institute (SMHI). https://sharkweb.smhi.se/hamta-data/. last accessed: 03 September 2022.
Steinmann, J.W., Grammer, G.M., Brunner, B., Jones, C.K., Riedinger, N., 2020. Assessing the application of trace metals as paleoproxies and a chemostratigraphic tool in carbonate systems: a case study from the “Mississippian Limestone” of the midcontinent, United States. Mar. Pet. Geol. 112 https://doi.org/10.1016/j.marpetgeo.2019.104061.
Sulu-Gambari, F., Seitaj, D., Behrends, T., Banerjee, D., Meysman, F.J., Slomp, C.P., 2016. Impact of cable bacteria on sedimentary iron and manganese dynamics in a seasonally-hypoxic marine basin. Geochim. Cosmochim. Acta 192, 49–69. https://doi.org/10.1016/j.gca.2016.07.028.
Sulu-Gambari, F., Roepert, A., Jilbert, T., Hagens, M., Meysman, F.J.R., Slomp, C.P., 2017. Molybdenum dynamics in sediments of a seasonally-hypoxic coastal marine basin. Chem. Geol. 466, 627–640. https://doi.org/10.1016/j.chemgeo.2017.07.015.
Sundby, B., Martinez, P., Gobeil, C., 2004. Comparative geochemistry of cadmium, rhenium, uranium, and molybdenum in continental margin sediments. Geochim. Cosmochim. Acta 68 (11), 2485–2493. https://doi.org/10.1016/j.gca.2003.08.011.
Sweere, T., van den Boorn, S., Dickson, A.J., Reichart, G.-J., 2016. Definition of new trace-metal proxies for the controls on organic matter enrichment in marine sediments based on Mn, Co, Mo and Cd concentrations. Chem. Geol. 441, 235–245. https://doi.org/10.1016/j.chemgeo.2016.08.028.
Taylor, S.R., McLennan, S.M., 1985. The Continental Crust : Its Composition and Evolution : An Examination of the Geochemical Record Preserved in Sedimentary Rocks, 12590231. Blackwell Scientific, Oxford, xv, 312 p pp.
Taylor, S.R., Mclennan, S.M., 1995. The Geochemical Evolution of the Continental-Crust. Rev. Geophys. 33 (2), 241–265. https://doi.org/10.1029/95rg00262.
Topcu, H.D., Brockmann, U.H., 2015. Seasonal oxygen depletion in the North Sea, a review. Mar. Pollut. Bull. 99 (1–2), 5–27. https://doi.org/10.1016/j.marpolbul.2015.06.021.
Tribovillard, N., 2020. Arsenic in marine sediments: how robust a redox proxy? Palaeogeogr. Palaeoclimatol. Palaeoecol. 550 https://doi.org/10.1016/j.palaeo.2020.109745.
Tribovillard, N., Riboulleau, A., Lyons, T., Baudin, F., 2004. Enhanced trapping of molybdenum by sulfurized marine organic matter of marine origin in Mesozoic limestones and shales. Chem. Geol. 213 (4), 385–401. https://doi.org/10.1016/j.chemgeo.2004.08.011.
Tribovillard, N., Algeo, T.J., Lyons, T., Riboulleau, A., 2006. Trace metals as paleoredox and paleoproductivity proxies: an update. Chem. Geol. 232 (1–2), 12–32. https://doi.org/10.1016/j.chemgeo.2006.02.012.
Tribovillard, N., Algeo, T.J., Baudin, F., Riboulleau, A., 2012. Analysis of marine environmental conditions based onmolybdenum–uranium covariation—applications to Mesozoic paleoceanography. Chem. Geol. 324-325, 46–58. https://doi.org/10.1016/j.chemgeo.2011.09.009.
Turekian, K.K., Wedepohl, K.H., 1961. Distribution of the elements in some Major units of the Earths Crust. Geol. Soc. Am. Bull. 72 (2), 175–191. https://doi.org/10.1130/0016-7606(1961)72[175:Doteis]2.0.Co;2.
Tyson, R.V., Pearson, T.H., 1991. Modern and Ancient Continental-Shelf Anoxia - an Overview. Geol. Soc. Spec. Publ. https://doi.org/10.1144/GSL.SP.1991.058.01.01. Statistics in medicine: 1-24.

Veeh, H.H., 1967. Deposition of uranium from the ocean. Earth Planet. Sci. Lett. 3, 145–150.

Virtasalo, J.J., Kohonen, T., Vuorinen, I., Huttula, T., 2005. Sea bottom anoxia in the Archipelago Sea, northern Baltic Sea—Implications for phosphorus remineralization at the sediment surface. Mar. Geol. 224 (1–4), 103–122. https://doi.org/10.1016/j.margeo.2005.07.010.

Vorlicek, T.P., Kahn, M.D., Kasuya, Y., Helz, G.R., 2004. Capture of molybdenum in pyrite-forming sediments: role of ligand-induced reduction by polysulfides. Geochim. Cosmochim. Acta 68 (3), 547–556. https://doi.org/10.1016/s0016-7037(03)00444-7.

Vorlicek, T.P., Helz, G.R., Chappaz, A., Vue, P., Vezina, A., Hunter, W., 2018. Molybdenum Burial Mechanism in Sulfidic Sediments: Iron-Sulfide Pathway. ACS Earth Space Chem. 2 (6), 565–576. https://doi.org/10.1021/acsearthspacechem.8b00016.

Wagner, M., Chappaz, A., Lyons, T.W., 2017. Molybdenum speciation and burial pathway in weakly sulfidic environments: Insights from XAFS. Geochim. Cosmochim. Acta 206, 18–29. https://doi.org/10.1016/j.gca.2017.02.018.

Wang, Z.M., Lee, S.W., Kapoor, P., Tebo, B.M., Giammar, D.E., 2013. Uraninite oxidation and dissolution induced by manganese oxide: a redox reaction between two insoluble minerals. Geochim. Cosmochim. Acta 100, 24–40. https://doi.org/10.1016/j.gca.2012.09.053.

van der Weijden, C.H., 2002. Pitfalls of normalization of marine geochemical data using a common divisor. Mar. Geol. 184 (3–4), 167–187. https://doi.org/10.1016/S0025-3227(01)00297-3.

Wignall, P.B., Myers, K.J., 1988. Interpreting benthic oxygen levels in mudrocks: a new approach. Geology 16 (5). https://doi.org/10.1130/0091-7613(1988)016<0452:Ibolim>2.3.Co;2.

Wijsman, J.W.M., Herman, P.M.J., Middelburg, J.J., Soetaert, K., 2002. A model for early diagenetic processes in sediments of the continental shelf of the Black Sea. Estuar. Coast. Shelf Sci. 54 (3), 403–421. https://doi.org/10.1006/ecss.2000.0655.

Yano, M., Yasukawa, K., Nakamura, K., Ikehara, M., Kato, Y., 2020. Geochemical Features of Redox-Sensitive Trace Metals in Sediments under Oxygen-Depleted Marine Environments. Minerals 10 (11). https://doi.org/10.3390/min10111021.

Yigiterhan, O., Murray, J.W., 2008. Trace metal composition of particulate matter of the Danube River and Turkish rivers draining into the Black Sea. Mar. Chem. 111 (1–2), 63–76. https://doi.org/10.1016/j.marchem.2007.06.019.

Zhang, S., Wang, X., Wang, H., Bjerrum, C.J., Hammarlund, E.U., Costa, M.M., Connelly, J.N., Zhang, B., Su, J., Canfield, D.E., 2016. Sufficient oxygen for animal respiration 1,400 million years ago. Proc. Natl. Acad. Sci. U. S. A. 113 (7), 1731–1736. https://doi.org/10.1073/pnas.1523449113.

Zheng, Y., Anderson, R.F., van Geen, A., Kuwabara, J., 2000. Authigenic molybdenum formation in marine sediments: a link to pore water sulfide in the Santa Barbara Basin. Geochim. Cosmochim. Acta 64 (24), 4165–4178. https://doi.org/10.1016/S0016-7037(00)00495-6.

Zheng, Y., Anderson, R.F., Van Geen, A., Fleisher, M.Q., 2002a. Preservation of particulate non-lithogenic uranium in marine sediments. Geochim. Cosmochim. Acta 66 (17), 3085–3092. https://doi.org/10.1016/S0016-7037(01)00632-9.

Zheng, Y., Anderson, R.F., Van Geen, A., Fleisher, M.Q., 2002b. Remobilization of authigenic uranium in marine sediments by bioturbation. Geochim. Cosmochim. Acta 66 (10), 1759–1772. https://doi.org/10.1016/S0016-7037(01)00886-9.